Hydroxysteroid dehydrogenase family proteins on lipid droplets through bacteria, *C. elegans*, and mammals

Yangli Liu[a,b,1], Shimeng Xu[a,1], Congyan Zhang[a,b,1], Xiaotong Zhu[a], Mirza Ahmed Hammad[a,b], Xuelin Zhang[c], Mark Christian[d], Hong Zhang[a,b], Pingsheng Liu[a,b,*]

[a] *National Laboratory of Biomacromolecules, CAS Center for Excellence in Biomacromolecules, Institute of Biophysics, Chinese Academy of Sciences, Beijing 100101, China*
[b] *University of Chinese Academy of Sciences, Beijing 100049, China*
[c] *School of Kinesiology and Health, Capital University of Physical Education and Sports, Beijing 100191, China*
[d] *Division of Metabolic and Vascular Health, Warwick Medical School, University of Warwick, Coventry, CV4 7AL, UK*

ABSTRACT

Lipid droplets (LDs) are the main fat storing sites in almost all species from bacteria to humans. The perilipin family has been found as LD proteins in mammals, *Drosophila*, and a couple of slime molds, but no bacterial LD proteins containing sequence conservation were identified. In this study, we reported that the hydroxysteroid dehydrogenase (HSD) family was found on LDs across all organisms by LD proteomic analysis. Imaging experiments confirmed LD targeting of three representative HSD proteins including ro01416 in RHA1, DHS-3 in *C. elegans*, and 17β-HSD11 in human cells. In *C. elegans*, 17β-HSD11 family proteins (DHS-3, DHS-4 and DHS-19) were localized on LDs in distinct tissues. In intestinal cells of *C. elegans*, DHS-3 targeted to cytoplasmic LDs, while DHS-9 labeled nuclear LDs. Furthermore, the N-terminal hydrophobic domains of 17β-HSD11 family were necessary for their targeting to LDs. Last, 17β-HSD11 family proteins induced LD aggregation, and deletion of DHS-3 in *C. elegans* caused lipid decrease. Independent of their presumptive catalytic sites, 17β-HSD11 family proteins regulated LD dynamics and lipid metabolism through affecting the LD-associated ATGL, which was conserved between *C. elegans* and humans. Together, these findings for HSDs provide a new insight not only into the mechanistic studies of the dynamics and functions of LDs in multiple organisms, but also into understanding the evolutionary history of the organelle.

1. Introduction

The excessive lipid storage in lipid droplets (LDs) is highly connected to metabolic diseases including obesity, atherosclerosis, hepatic steatosis, insulin resistance, and hyperlipidemia [1–3]. LDs are the intracellular storage site for neutral lipids and have been found in almost all eukaryotic cells, and some prokaryotic cells, such as *Rhodococcus* [4–6]. All LDs share the same basic structure consisting of a hydophobic core of neutral lipids (triacylglycerol (TAG) and sterol ester (CE)), which is wrapped by a monolayer of phospholipids decorated by proteins. The composition of neutral lipids, phospholipids and proteins varies among organisms and tissues [7]. The lipids in LDs function as metabolic substrates for energy production and as components for membrane synthesis in cells [8].

Numerous studies have identified several resident proteins on the LD surface [9–12]. These proteins are involved in lipid metabolism and transport, membrane trafficking, and chaperone function [13–16]. The protein composition varies among subpopulations of LDs within a cell, or between LDs isolated from different cell types. The best known examples of LD resident proteins are the perilipins. They have been proposed to serve structural roles on the LD surface and have been found to regulate cellular lipid metabolism and play significant roles in human health [17,18]. Perilipins were first identified in mammals. Their homologs were subsequently found in *Drosophila* and a few slime molds such as *Dictyostelium* based on sequence homology [17,19,20]. However, similar bioinformatic approaches failed to identify perilipin homologs in other organisms including *C. elegans,* plants, yeast and bacteria. This raises the question on the existence of evolutionarily conserved LD proteins that are present from bacteria to humans.

Using newly developed techniques, LDs have been isolated from many cell types and tissues of almost all model biological organisms and analyzed by proteomic techniques [5,11,21,22]. These studies

---

reveal that a large set of hydroxysteroid dehydrogenases (HSDs) is targeted to LDs. HSDs, which belong to the superfamily of short-chain dehydrogenases/reductases (SDRs) or aldo-ketoreductases (AKRs), are important enzymes involved in lipid metabolism and especially in steroid hormone metabolism. Evolutionarily, the SDR protein family is ancient, and is found in all forms of life, including bacteria and archaea, providing clues to their fundamental significance in metabolic processes [23–26]. This broadly conserved family may provide insight into the evolution of LD as an organelle.

The mechanisms governing the targeting of LD proteins are still not well understood. The subcellular localization of perilipins and other LD-associated proteins varies between cell types and tissues and the LD targeting pattern can differ even within a cell [27,28]. In this study, we enumerate LD targeting patterns, the cellular distribution and the correlation of cellular distribution with functional significances of HSDs.

In mammals, SDRs function as enzymatic switches controlling the balance between active and inactive steroid hormones. By binding to specific receptors, steroids exert transcriptional control over numerous genes that regulate physiological processes including cell signaling, growth, reproduction, and energy homeostasis. For example, the SDR enzymes RDH10 and DHRS3 contribute to the oxidation of retinol in the retinoic acid biosynthetic pathway, thus playing an important role in embryonic development [29,30]. Although these two proteins have been found on LDs, the significance of this localization to their functions is not clear [31,32].

One typical class of SDRs, the 17β-hydroxysteroid dehydrogenases (17β-HSDs), catalyzes the oxidation or reduction at position 17 in the D ring of steroids, and is primarily involved in estrogen and androgen synthesis [33]. These hormones stimulate and control the development and maintenance of female and male characteristics and other processes. Besides their role in sex hormone formation, a few 17β-HSD enzymes, such as 17β-HSD3 and 17β-HSD12, are involved in fatty acid production and are essential for growth, reproduction and development in *C. elegans* [34,35]. The role of LD resident 17β-HSDs in the integration of sex hormone synthesis and lipid metabolism requires further investigation.

In the 1990s, it was reported that oral estrogen treatment was associated with increased body fat [36]. Subsequent evidence indicated that estrogen depressed whole body lipid oxidation and increased adiposity, possibly through regulation of carnitine palmitoyl-transferase-1 (Cpt 1) expression [37,38]. The underlying mechanism linking estrogenic regulation of lipid metabolism was thought to depend on interactions of estrogen receptor signaling events involving lipolytic and/or lipogenic enzyme activity, free fatty acid metabolism, and adipokine production. For example, estrogen receptor alpha (ERα) could regulate lipid metabolism in bone through ATGL and perilipin, and ACSL4 was a target of 17β-estradiol-stimulated ERα and was required for the cellular uptake of exogenous PUFA in ERα positive breast carcinoma cells [39–41]. These findings raise the question: whether LD associated HSDs are involved in the formation of estrogen, androgen or other steroid hormones which subsequently regulate lipid metabolism and other cellular processes. For example, 17β-HSD13 was identified as a liver-specific LD-associated protein which contributed to the pathogenesis of nonalcoholic fatty liver disease (NAFLD) by an unknown mechanism [12,42].

In this study, we report deep conservation of LD targeting by HSD proteins in different organisms, and different tissues and distributions in the intestinal cells of *C. elegans*. In addition, *C. elegans* DHS-3 and its mammalian ortholog 17β-HSD11 regulate LD size, LD distribution and TAG content similar to that seen with ATGL, but in a manner independent of their putative catalytic sites. These data indicate that the significance of HSDs, a conserved LD protein family.

2. Materials and methods

2.1. Plasmids, strains and culture conditions

The bacterial *Rhodococcus sp.* RHA1 (RHA1) strain was used as wild type and for genetic mutants. The transgenic RHA1 bacteria used in this study are listed (Table S1). The ro01416 gene deletion mutant was constructed as described in a previous study [5]. Cells of RHA1 were cultivated aerobically in LB at 30 °C. Then 1 ml of cells (OD$_{600}$ = 2.0) was collected by centrifugation and then cultured in 10 ml mineral salt medium (MSM) with 0.5 g/l NH$_4$Cl and 10 g/l sodium gluconate until reaching OD$_{600}$ = 2.0–2.5. The culture conditions were as described previously [5,43].

The N2 Bristol strain of *C. elegans* was used as wild type in this study. The genetic mutants, transgenic worms and RNAi bacteria strains used are listed (Table S1). Nematode growth media was used to maintain *C. elegans* with the *E. coli* strain (OP50) as food at 20 °C.

HeLa cells were cultured in DMEM (Macgene Biotech., Beijing, CN) supplemented with 10% FBS (Hyclone), 100 U/ml penicillin and 100 mg/ml streptomycin (Macgene Biotech., Beijing, CN) at 37 °C with 5% CO$_2$. Sodium oleate (OA) (Sigma-Aldrich) was prepared as described previously [44]. Cells were treated with OA (+OA) in culture medium and absolute ethanol was used as vehicle control. Transgenic cells are listed (Table S1).

All the plasmids used in this study are also listed in Table S1. Plasmid pGEX-6P-2 and pET28a-SMT3 were used for protein expression in *E. coli*, pJAM2 for protein expression in RHA1, pK18mobsacB for gene knockout in RHA1, pPD95.79 and pPD49.26 for protein expression in *C. elegans*, and pEGFP-N1 and pQCXIP for protein expression in HeLa cells.

2.2. Staining and image analysis

Cultured RHA1 cells were collected and washed twice with PBS. Then cells were applied to glass coverslips pretreated with poly-L-lysine (PB0589) and dried for 30 min. The coverslips were washed three times with 1 ml PBS and were incubated with LipidTOX red (diluted 1:500 in PBS), protected from light, for 30 min. The stained samples were mounted on glass slides using mounting media (P0126) and were visualized with an Olympus FV1000 confocal microscope.

L4 worms were washed off growth plates and were washed three times with PBS. Then worms were fixed in 4% paraformaldehyde for 30 min. Fixed worms were washed three times, and stained with LipidTOX red (1:1000). Worms were laid on a 6% agar plate, washed three times and were visualized by confocal microscopy.

HeLa cells on glass coverslips were fixed in 4% paraformaldehyde for 30 min and were washed three times with PBS. LDs and nuclei were stained separately by LipidTOX red and Hoechst for 30 min protected from light. The stained cells were washed three times, mounted with Mowiol mounting media and were then examined by confocal microscopy.

2.3. Isolation of lipid droplets and protein preparation for Western blotting

Cultured RHA1 and HeLa cells were collected and fractionated as described previously [5,45]. Worms were washed and fractionated as described previously [11].

The proteins in different fractions were separated on 10% SDS-PAGE gels followed by silver staining or Western blotting. Polyclonal antibodies for DHS-3 and MDT-28/PLIN-1 were prepared by AbMax Biotechnology Co., Ltd. The anti-GFP (IMA1006L, IMAGEN), anti-GST (IMA1002L, IMAGEN), anti-Actin (HX1827, Hua Xin Bo Chuang), anti-GAPDH (MAB374, Millipore), anti-ATGL (2138 s, Cell Signaling), anti-PLIN2 (610,102, Progen) and anti-17β-HSD11 (ab136109, Abcam) were purchased.

2.4. Expression and purification of proteins

Standard molecular cloning techniques were used. Ro01416 and DHS-3 were cloned into the pGEX-6 P-2 expression vector and were expressed with an N-terminal GST tag. GFP and 17β-HSD11 was cloned into the pET28a-SMT3 expression vector and was expressed with an N-terminal 6×His tag and SMT3 domain.

All of the proteins were expressed in Rosetta *E. coli* in LB media. The cells were grown to an OD600 of 0.6 and were induced with 0.4 mM isopropyl β-D-1-thiogalactopyranoside (IPTG) at 16 °C for 24 h. The cells were collected by centrifugation at 4000 g for 20 min. Then the cells expressing GST-ro01416 and GST-DHS-3 were resuspended in 50 mM Tris-HCl, 150 mM NaCl, 1 mM EDTA, 1 mM DTT and 4% Glycerol (pH 7.4) while the cells expressing HIS-SMT3-17β-HSD11 and HIS-SMT3-GFP were resuspended in 50 mM Tris-HCl, 150 mM NaCl (pH 7.4). Cells were then lysed in a high-pressure cell press (JNBIO JN-3000 PLUS) and the cell lysates were centrifuged at 16, 000 g for 1 h to obtain clarified supernatants. The supernatants containing soluble GST-ro01416, GST-DHS-3 proteins were applied to GST affinity chromatography resin (Glutathione sepharose 4B, GE), and the supernatants of soluble HIS-SMT3-GFP and HIS-SMT3-17β-HSD11 protein were applied to nickel affinity chromatography resin (Chelating Sepharose Fast Flow, Amersham Biosciences). The chromatographic purifications were completed according to manufacturer's guidelines. The GSH and imidazole used to elute the proteins were removed by buffer exchange using Amicon centrifugal concentrators (Millipore). The GFP and 17β-HSD11 proteins were obtained from the cleavage of HIS-SMT3-GFP and HIS-SMT3-17β-HSD11 by SUMO protease ULP1. The purity of the proteins was detected by SDS–PAGE.

2.5. Construction of adiposomes and recruitment of proteins to adiposomes

The construction of adiposomes and the experiments involving the recruitment of proteins to adiposomes were conducted as described previously [46]. 1,2-Di (9Z-octadecenoyl)-sn-glycero-3-phosphocholine (DOPC) was purchased from Avanti and the TAG used was extracted from rat fat pads in the laboratory. Defined quantities of purified proteins were added to adiposomes to a final volume of 60 μl. The mixture was gently vortexed and then incubated at room temperature for 1 h. The adiposomes were centrifuged at 15, 000 rpm for 5 min and the solution was removed for analysis. Equal amount of proteins, adiposomes and solutions were analyzed by SDS-PAGE.

2.6. Measurement of TAG and cholesterol ester (CE) levels

RHA1 cells, worms and HeLa cells were washed three times with PBS, and were then dissolved in 200 μl 1% Triton X-100 with sonication. Whole cell lysates were centrifuged at 15, 000 rpm for 5 min at 4 °C. The TAG and CE content of the supernatants were separately measured using the Triglyceride Assay Kit and CHO Assay Kit (BioSino Bio-Technology and Science Inc., China). The corresponding protein concentration was quantified using a Pierce BCA Protein Assay Kit (Thermo, USA).

2.7. Growth rate and fertility analysis

Eggs isolated from gravid adults using hypochlorite treatment were hatched in M9 buffer overnight, and were then plated onto NGM plates. The number of worms that reached adult stage was scored 2 days later. Then, 5 L4 worms were transferred individually to fresh plates. Worms were transferred daily until they did not produce any more progeny. Two or three days after removal of the adult, the number of live progeny was counted. Line charts and histograms were made with Graphpad prism 5.

2.8. Quantitative RT-PCR analysis

Total RNA was isolated using Trizol reagent according to the manufacturer's protocol. cDNA was synthesized using Moloney murine leukemia virus (M-MuLV) reverse transcriptase with random hexamer primers. RT-PCR was performed on a CFX96 real-time system with SYBR green. Relative expression levels of all mRNAs were normalized to *ama-1* mRNA.

2.9. Statistical analyses

Data are presented as mean ± SEM unless otherwise indicated. The statistical analyses were performed using GraphPad Prism 6 and Image J (NIH, USA). Determination of significance between groups was performed using Student *t*-tests, or Two-way ANOVA as indicated.

3. Results

3.1. HSD proteins are present in the LD proteomes of almost all cell types and organisms

There have been numerous studies examining the proteomes of LDs from diverse cell types and tissues of organisms including bacteria, green algae, yeast, plants, worms, insects, and mammals. HSD family members have been identified on LDs in many of these studies as summarized in Table 1 and Table S2. The variations in the nomenclature for HSD proteins are presented for reference in Table S3. The SDR proteins that have been found in various LD proteomes are summarized in Table S4.

3.2. 17β-HSD11 family proteins are localized on LDs from bacteria, C. elegans and mammals

As shown in Table 1, 17β-HSD11 subfamily members are frequently found on LDs. These proteins are highly conserved among bacteria, yeast, worms, insects, mice, and humans as demonstrated by sequence alignment (Fig. 1A). Here, we use *Rhodococcus jostii* RHA1, *C. elegans* and HeLa cells to determine the localization of HSD proteins.

In bacteria, three HSD proteins, ro03952 (ortholog of 17β-HSD10), ro06007 (ortholog of 17β-HSD11) and ro01416 (ortholog of 17β-HSD12) were identified in LD proteomes (Table S2). To confirm the localization of these three proteins by an independent method, GFP fusion proteins were expressed in RHA1. The transfected cells were stained with LipidTOX red and were visualized by confocal microscopy. The images showed no colocalization of LipidTOX with ro03952-GFP and ro06007-GFP (data not shown), suggesting that these proteins are not located on LDs, or that GFP disrupts their targeting. However, ro01416-GFP was clearly colocalized with LDs (Fig. 1Ba). For further confirmation, the ro01416-GFP strain was fractionated by differential centrifugation and the fractions were separated by SDS-PAGE. The ro01416-GFP protein was found in the LD fraction as shown by Western blotting (Fig. 1Bb). Therefore, ro01416 is localized to LDs in RHA1 while the other two family members are not.

In *C. elegans*, the protein DHS-3, the ortholog of 17β-HSD11, was specifically localized on LDs as demonstrated by both morphological and biochemical methods (Fig. 1Ba, Bb). This is in agreement with our previous work [11,75]. When human 17β-HSD11-GFP was expressed in HeLa cells, it also colocalized with LipidTOX signals (Fig. 1Ba). In addition, in untransfected HeLa cells, endogenous 17β-HSD11 was detected in LDs by Western blotting (Fig. 1Bb), which was consistent with previous findings [49,71].

To verify these results, additional *in vitro* experiments were conducted. We have reported that recombinant LD-associated proteins could be recruited to adiposomes constructed *in vitro* [46]. Recombinant GST-ro01416, GST-DHS-3 and 17β-HSD11 were expressed in and purified from *E. coli*. These recombinant proteins were incubated

Table 1
Summary of HSDs in LD proteomes.

Proteins	LD types		References
	Organisms	Tissues and cells	
3β-HSD1	Mouse; human	Intestine cells; steroidogenic cells	[47–50]
3β-HSD2	/	/	
3β-HSD3	/	/	
3β-HSD4	Rat	Liver	[51]
3β-HSD5	Rat	Liver	[51]
3β-HSD6	/	/	/
3β-HSD7	Mouse; Rat	Skeletal muscle (cells); Pancreatic β-cells	[10,52]
11β-HSD1	Plants; mouse; human	BAT; liver;	[12,53–58]
11β-HSD2	/	/	/
11β-HSD3	/	/	/
17β-HSD1	Yeast		[59,60]
17β-HSD2	Yeast; human	Liver; intestine cells	[12,48,61]
17β-HSD3	/	/	/
17β-HSD4	Mouse; rat; human	BAT; liver; WAT; skeletal muscle (cells); hepatocytes; pancreatic β-cells	[10,12,52,53,62,63]
17β-HSD5	/	/	/
17β-HSD6	Human	Liver	[12]
17β-HSD7	Yeast; Mouse; Rat; Human	Liver; skeletal muscle (cells); adipocytes; epithelia; fibroblasts; intestine cells; macrophage; pancreatic β-cells; steroidogenic cells	[9,10,12,47,49,51,52,61,64–68]
17β-HSD8	Mouse	BAT	[53]
17β-HSD9	/	/	/
17β-HSD10	Bacteria; Insects; mouse	BAT; steroidogenic cells	[5,49,53,69]
17β-HSD11	Bacteria; worms; insects; mouse; rat; human	Liver; skeletal muscle (cells); epithelia; fibroblasts; hepatocytes; intestine cells; steroidogenic cells	[4,9–12,21,47–49,65,70–74]
17β-HSD12	Worms; bacteria; mouse; human	Liver; skeletal muscle cells	[4,10–12]
17β-HSD13	Rat; human	Liver	[12,51]
17β-HSD14	Yeast		[61]

with adiposomes, the mixture was centrifuged, and the solution containing unbound proteins was removed (Fig. S1a). Fractions from the separation were examined by silver staining and Western blotting. These analyses demonstrated that ro01416 was partially targeted to the adiposomes, and that DHS-3 and 17β-HSD11 localized to adiposomes (Fig. S1b). This finding indicated that these three proteins could target to LDs without interactions with any other proteins. Together, these results reveal that 17β-HSDs in bacteria, *C. elegans* and mammals all target to LDs (Fig. 1C).

3.3. DHS-3 and its paralogs, DHS-4 and DHS-19, are localized on LDs in different tissues in C. elegans

In *C. elegans*, the DHS family members DHS-3, DHS-4, DHS-9 and DHS-19 were found in the LD proteome (Table S2). Based on the small phylogenetic tree, DHS-3, DHS-4 and DHS-19 are closely related, and all of them are predicted to be orthologs of 17β-HSD11 (Fig. 2A and Table S5). To examine the cellular distribution and localization of DHS-4 and DHS-19, transgenic *dhs-4p::dhs-4::gfp* and *dhs-19p::dhs-19::gfp* animals were generated. The *dhs-3p::dhs-3::gfp* animals were generated in our laboratory previously. The localizations of the GFP fusion proteins were observed within the living animals using confocal microscopy. DHS-3 (Fig. 2B, arrow) has been determined to be mainly localized on intestinal LDs [75]. Based on the morphology, DHS-4 was detected in the hypodermis (Fig. 2B, arrows). DHS-19 was also in the hypodermis, as well as possibly localized on LDs in the muscle (Fig. 2B, arrows). In addition, DHS-4 and DHS-19 were present on ring-like structures, typical for LD localized proteins. To further verify the LD localization of these GFP fusion proteins, the previously identified LD protein MDT-28/PLIN-1::mCherry was introduced to these three reporters and was visualized by confocal microscopy. All GFP signals were observed to be colocalized with the mCherry signals (Fig. S2), directly demonstrating their subcellular localization to LDs.

3.4. DHS-9::GFP labels nuclear LDs in C. elegans and Huh7 cells

DHS-9 is predicted to be an ortholog of DHRS1 (which has been

identified in a LD proteomics study), and is part of a subfamily of the SDR superfamily (Table. S4). To examine the expression pattern and cellular functions of DHS-9, DHS-9::GFP driven by its endogenous promoter was constructed. We observed that the GFP tagged protein was expressed in the intestine, and was found at high levels in the nucleus and at lower levels in the cytosol (Fig. 2C). Besides the diffuse GFP signals in the nucleus, additional GFP puncta were found in the nucleoplasm of some, if not all, nuclei of intestinal cells (Fig. 2C). We further examined the punctate structures by confocal microscopy. Interestingly, micrographs of confocal microscopy with airyscan clearly showed clustered rings (Fig. 2D). Thus DHS-9 appears to form clustered rings in nuclei.

To determine if the structures labeled by DHS-9 were nuclear LDs, we examined whether the previously identified LD protein DHS-3 and MDT-28/PLIN-1 could colocalize with DHS-9 in the nucleus. Thus, *dhs-9p::dhs-9::gfp; dhs-3p::dhs-3::mCherry*, and *dhs-9p::dhs-9::gfp; mdt-28/ plin-1p::mdt-28/plin-1::mCherry* worms were constructed and examined by confocal microscopy. The fluorescence images showed no colocalization of DHS-3::mCherry or MDT-28/PLIN-1::mCherry with DHS-9::GFP in the nucleus (Fig. S3a, Fig. S3b). Instead, DHS-3 and MDT-28/ PLIN-1 were exclusively present on the cytoplasmic LDs. In another experiment, MDT-28/PLIN-1 was expressed with a nuclear localization signal to examine whether MDT-28/PLIN-1 colocalize with DHS-9 in the nucleus. Transgenic animals expressing *mdt-28/plin-1p::mdt-28/plin-1::mCherry::NLS; dhs-9p::dhs-9::gfp* worms were generated and we observed MDT-28/PLIN-1::mCherry::NLS colocalized well with DHS-9::GFP in the nucleus (Fig. 2E).

The DHS-9::GFP signal was also found in the cytosol (Fig. 2C). However, the signal was very weak, which made observation of specific LD targeting difficult. Therefore, to verify whether DHS-9::GFP could target to cytoplasmic LDs, LDs from *dhs-9p::dhs-9::gfp* worms were purified and examined microscopically. GFP signal was found on the purified LDs. In parallel, LDs from *dhs-9p::dhs-9::gfp; mdt-28/plin-1p::mdt-28/plin-1::mCherry* worms were purified and the images also showed GFP signal colocalized with mCherry signal (Fig. 2F, Fig. S3c), suggesting DHS-9 could target to cytoplasmic LDs.

Nuclear LDs were observed previously in Huh7 cells [76].
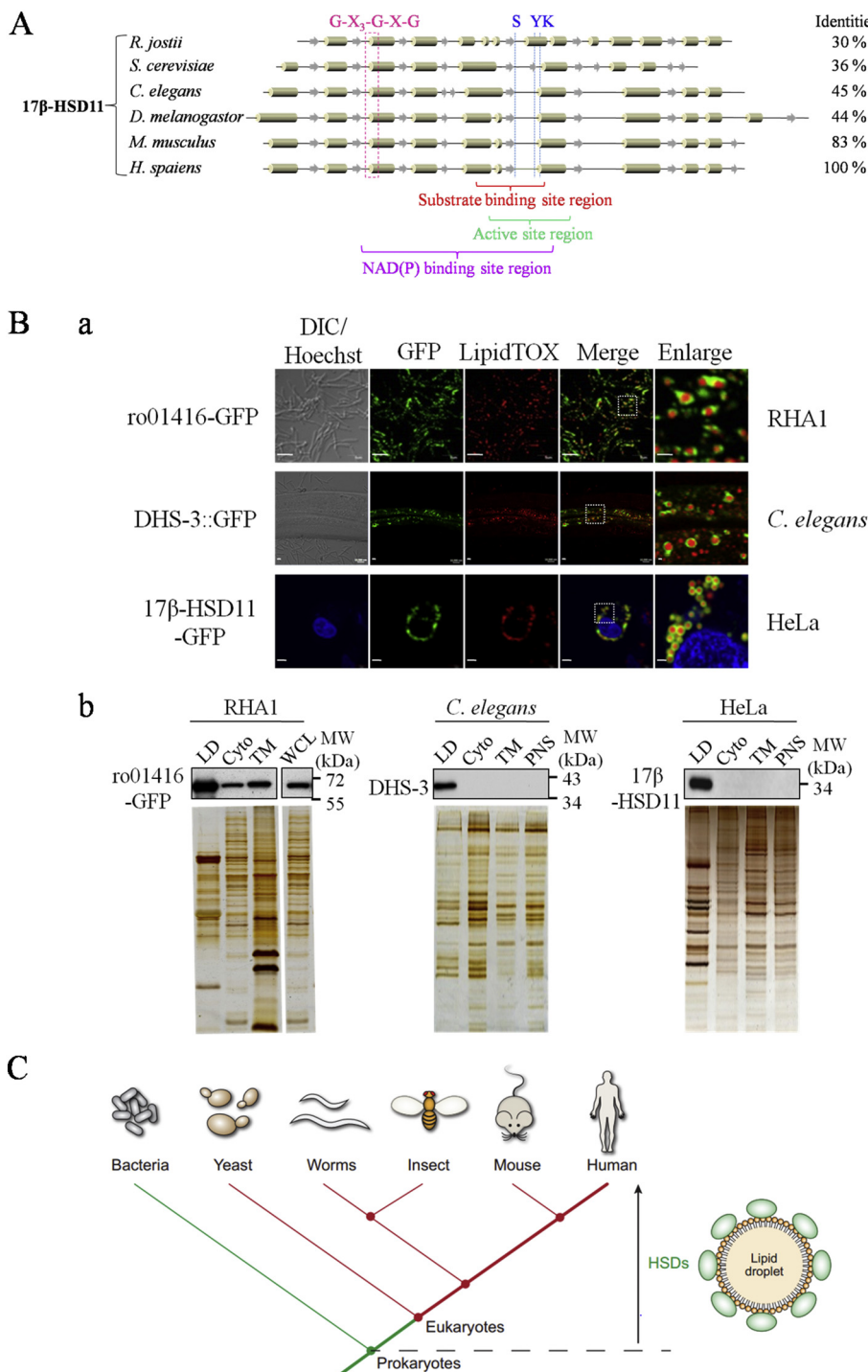
Fig. 1. 17β-HSD11 family proteins were localized on LDs of bacteria, *C. elegans* and mammalian cells.
(A) 17β-HSD11 family members have similar predicted structural features and sequences. This cartoon compares the structures of six members of the 17β-HSD11 family. From top to bottom, the sequences are ABG97784.1 from *Rhodococcus jostii,* Q05016.1 from *Saccharomyces cerevisiae,* NP_001122508.1 from *Caenorhabditis elegans,* NP_001260655.1 from *Drosophila melanogaster,* Q9EQ06.1 from *Mus musculus* and Q8NBQ5.3 from *Homo sapiens.* The secondary structural elements are predicted using Psipred. α-helices are indicated with cylinders, and β-strands with arrows. The Gly-X3-Gly-X-Gly motif, Ser (S), Tyr (Y), and Lys (K) residues are labeled. Substrate binding site regions, active site regions and NAD(P) binding site regions as predicted in NCBI are indicated. The percent identities represent the alignment of each sequence with Q8NBQ5.3 from *Homo sapiens* using blast in NCBI. (B) (a) Confocal microscopy images of LD localization of ro01416-GFP in RHA1, DHS-3::GFP in *C. elegans* and 17β-HSD11-GFP in HeLa cells. The green ring-like structures are due to LD targeting of these three GFP fusion proteins. LDs were stained by LipidTOX (red). Scale bar, 5 μm. Enlarged images: scale bar, 1 μm. (b) ro01416-GFP-expressing bacteria, wild type *C. elegans* and HeLa cells were fractionated and proteins from isolated lipid droplets (LD), cytosol (Cyto), total membrane (TM), post-nuclear supernatant (PNS) and whole cell lysates (WCL) were separated by 10% SDS-PAGE followed by silver staining or were analyzed by Western blotting with anti-GFP, anti-DHS-3 and anti-17β-HSD11, separately. (C) This cartoon depicts LD targeting of HSDs from prokaryotes (bacteria) to eukaryotes (yeast, worms, insects, mice and humans).

Therefore, DHS-9::GFP was transfected into Huh7 cells to investigate whether the protein would target to nuclear LDs in mammalian cells. Under standard culture conditions, the GFP signal was diffusely distributed. However, when the cells were treated with 200 μM OA, the DHS-9::GFP partially colocalized with LipidTOX red staining in the cytosol and nucleus (Fig. 2G), demonstrating that DHS-9 can be targeted to mammalian LDs in both the cytosol and the nucleus. Similar results were seen with DHRS1, the ortholog of DHS-9 in humans (Fig. 2G).

Together, these results show that DHS-3, DHS-4 and DHS-19 are localized on LDs in different tissues. Furthermore, for DHS-9, the targeting probably extends to nuclear LDs in the intestine of *C. elegans*

(Fig. 2H) but a definite answer will require more sensitive tests in the future.

3.5. LD targeting of DHS-3 and 17β-HSD11 is retained in divergent eukaryotic organisms

We next examined whether LD targeting of 17β-HSD proteins was broadly conserved. First, the subcellular localization of DHS-3 in HeLa cells and that of 17β-HSD11 in *C. elegans* was determined. DHS-3-GFP was transfected in HeLa cells and the protein showed perfect colocalization with LDs (Fig. 3Aa). Next, transgenic *C. elegans* that expressed 17b-HSD11 under the control of an intestinal-specific promoter was
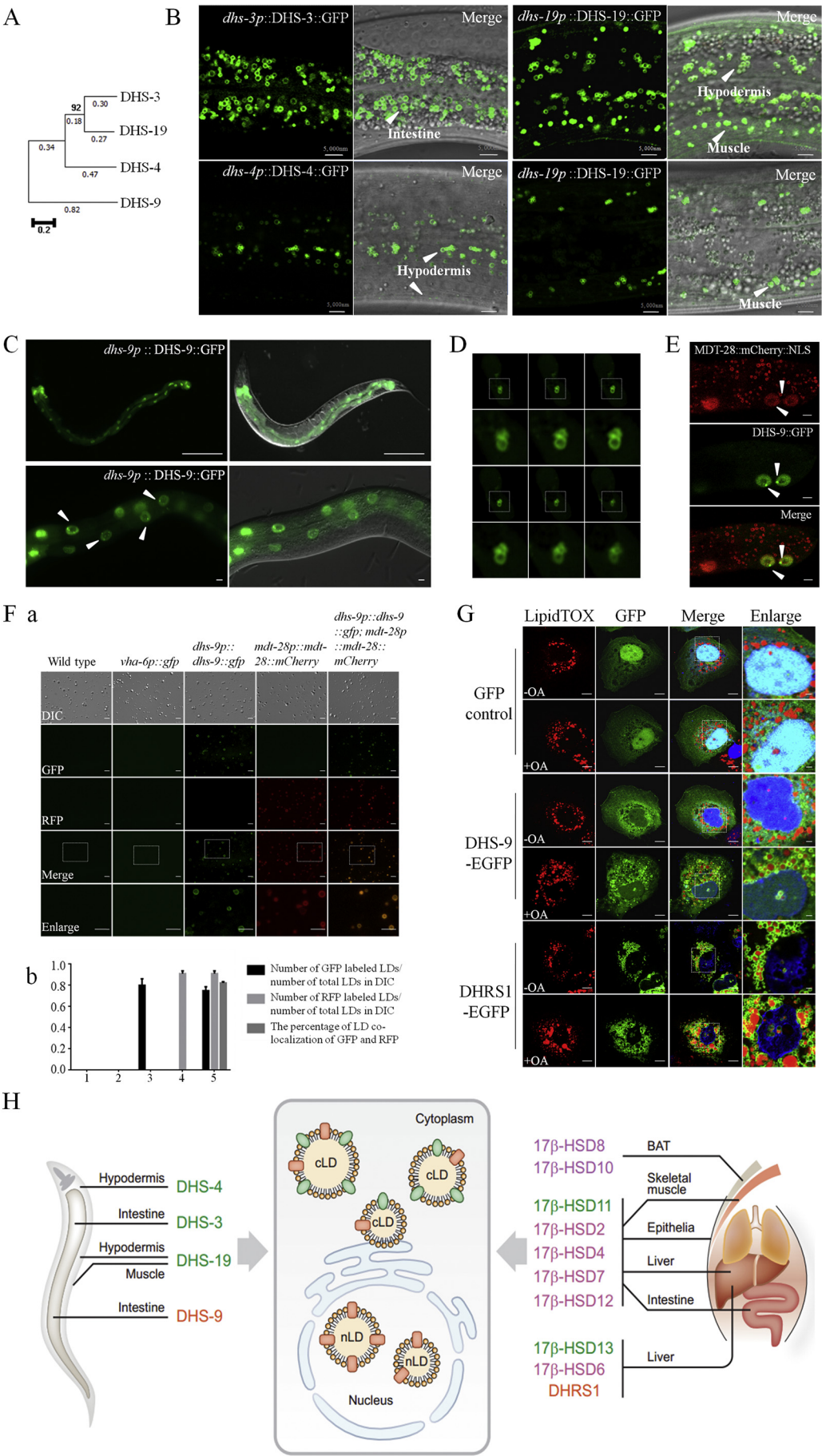
Fig. 2. HSDs were localized on LDs in specific tissues and different cellular structures of individual cells in *C. elegans*.

(A) Phylogeny of HSDs in LD proteome of *C. elegans*, including DHS-3, DHS-4, DHS-9 and DHS-19. (B) Tissue distribution of DHS-3, DHS-4 and DHS-19. Confocal micrographs of expression patterns of these three proteins in larval L4 stage animals: *dhs-3p*::DHS-3::GFP in the intestine, *dhs-4p*::DHS-4::GFP in the hypodermis, and *dhs-19p*::DHS-19::GFP in the hypodermis and muscle as indicated by the arrows. Scale bar, 5 μm. (C) Cellular distribution of DHS-9. Fluorescence micrographs of *dhs-9p*::DHS-9::GFP in larval L4 stage animals. The upper images: scale bar, 100 μm. The lower images: GFP fluorescence in the nucleus is indicated by the arrow. Scale bar, 5 μm. (D) Micrographs of confocal LSM880 with airyscan showed *dhs-9p*::DHS-9::GFP in different optical slices from top to bottom (from left to right, from upper to lower). It allowed images to be taken with a higher resolution than the diffraction limit. (E) Confocal micrographs of MDT-28/PLIN-1::mCherry::NLS and DHS-9::GFP in a young adult animal. Colocalization of RFP and GFP signals in the nucleus is indicated by arrows. Scale bar, 5 μm. (F) (a) Fluorescence micrographs of isolated LDs in wild type (1), *vha-6p::gfp* (2), *dhs-9p::dhs-9::gfp* (3), *mdt-28/plin-1p::mdt-28/plin-1::mCherry* (4) and *dhs-9p::dhs-9::gfp; mdt-28/plin-1p::mdt-28/plin-1::mCherry* (5) animals. Scale bar, 5 μm. Enlarged images: scale bar, 5 μm. (b) Quantification of images in (a). (G) Confocal micrographs of LD localization of DHS-9 and DHRS1 in Huh7 cells. GFP control, DHS-9-GFP (NP_498146.1) and DHRS1-GFP (Q96LJ7.1) were transfected into Huh7 cells with OA (+OA) or without OA (−OA) treatment. LDs were stained with LipidTOX (red) and the nucleus by Hoechst (blue). Scale bar, 5 μm. Enlarged images: scale bar, 1 μm. (H) The Cartoon shows HSDs are localized on LDs in different tissues and on different types of LDs. DHS-3, DHS-4 and DHS-19 (green) are separately localized on cytoplasmic LDs in intestine, hypodermis, hypodermis and muscle. The human ortholog 17β-HSD11 (green) was in several tissues, while 17β-HSD13 was restricted to the liver. Other 17β-HSDs (purple) were found in the LD proteomes of different tissues (not yet validated by additional experimental data). DHS-9 and its human homolog DHRS1 (orange) are localized on cytoplasmic LDs and nuclear LDs in the intestine of *C. elegans* and liver cells of mammals.
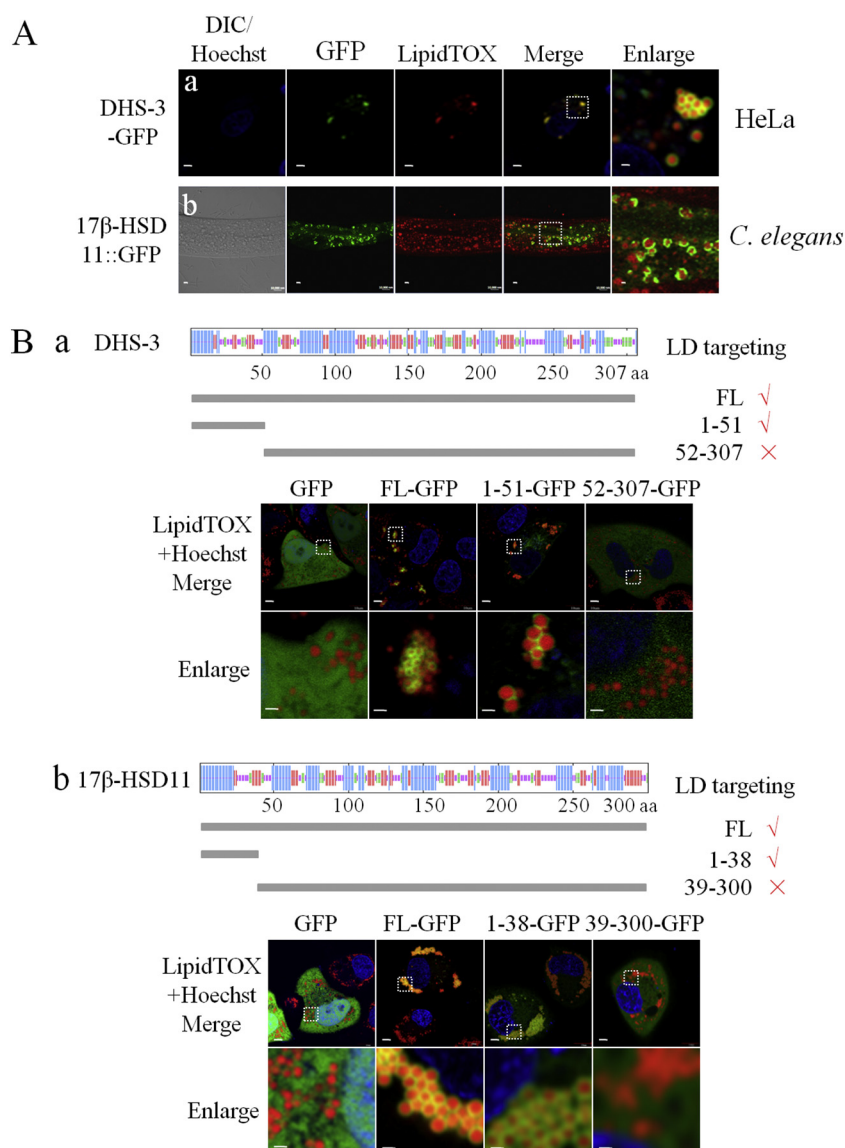
Fig. 3. DHS-3 and 17β-HSD11 targeted to LDs in diverse eukaryotic organisms, and N-terminal hydrophobic domains were necessary for their association with LDs.

(A) Confocal micrographs showing LD localization of DHS-3-GFP in HeLa cells (a) and 17β-HSD11::GFP in *C. elegans* (b). DHS-3-GFP was transfected into HeLa cells and *vha-6p::17β-HSD11::GFP* transgenic animals were generated. LDs were stained by LipidTOX (red). Scale bar, 5 μm. Enlarged images: scale bar, 1 μm. (B) LD targeting sequences of DHS-3 and 17β-HSD11. Truncations of DHS-3 (a) and 17β-HSD11 (b) were made based on secondary structure predictions (α helices indicated with blue vertical lines; β strands with red vertical lines and β turns with light green vertical lines). Constructs coding for the full length proteins and truncations of DHS-3 and 17β-HSD11 were fused with GFP, expressed in HeLa cells and co-imaged with LipidTOX red staining using confocal microscopy. Scale bar, 5 μm. Enlarged images: scale bar, 1 μm.

generated. The *vha-6p*::17β-HSD11::GFP was observed surrounding the LipidTOX signal in fixed worms (Fig. 3Ab). Together, these results clearly demonstrate that DHS-3 and 17β-HSD11 can target to LDs in diverse eukaryotic models.

However, when ro01416-GFP was transfected in *C. elegans* and HeLa cells, we only observed diffuse GFP in the cytosol. Similarly, when DHS-3-GFP and 17β-HSD11-GFP were transfected into RHA1 cells, diffused fluorescence patterns were observed (data not shown).

3.6. The N-terminal hydrophobic domains of DHS-3 and 17β-HSD11 are necessary for their association with LDs

To examine the mechanisms driving LD localization of the 17β-HSDs in different organisms, truncation mutants were prepared based on their secondary structures. GFP-fusion truncations of DHS-3 (amino acids 1–51 and 52–307) and that of 17β-HSD11 (amino acids 1–38 and 39–300), as well as their full-length proteins were constructed and then expressed in HeLa cells. The results showed that the full-length and 1–51 fragment of DHS-3 as well as the full-length and 1–38 fragment of 17β-HSD11 were colocalized with LDs (Fig. 3B). However, the 52–307 fragment of DHS-3 and 39–300 fragment of 17β-HSD11 were restricted to the cytosol, indicating that the N-termini of these two proteins were necessary for LD targeting.

A similar experiment was conducted with the bacterial ro01416. GFP-fusion fragments (amino acids 1–60, 1–223, 61–267, 100–267, 144–267, 197–267 and 224–267) and the full-length protein were generated and were expressed in RHA1 cells. Analysis by confocal microscopy showed that the full-length and fragments of 61–267, 100–267, and 144–267 were colocalized with LipidTOX signal, and the 197–267 fragment was partially colocalized with LDs. In contrast, the 1–60, 1–223 and 224–267 fragments were distributed in the cytosol, indicating that the C-terminus of ro01416 was necessary for its targeting to LDs (Fig. S4a).

The alignment of LD targeting sequences, including C-terminus of ro01416 (144–267), and N-termini of DHS-3 (1–51) and 17β-HSD11 (1–38), showed that the LD targeting sequences of DHS-3 and 17β-HSD11 were more similar to each other than either was to the ro01416 C-terminus (Fig. S4b).

3.7. Exogenous expression of DHS-3 and 17β-HSD11 induces LD aggregation and elevated TAG levels

We next examined the functions of DHS-3 and 17β-HSD11. Overexpression of DHS-3 in *C. elegans* induced LD clustering (Fig. 2B). Examination of a *vha-6p::dhs-3::gfp* single copy worm showed GFP signal on relatively dispersed LDs. We speculate that the expression
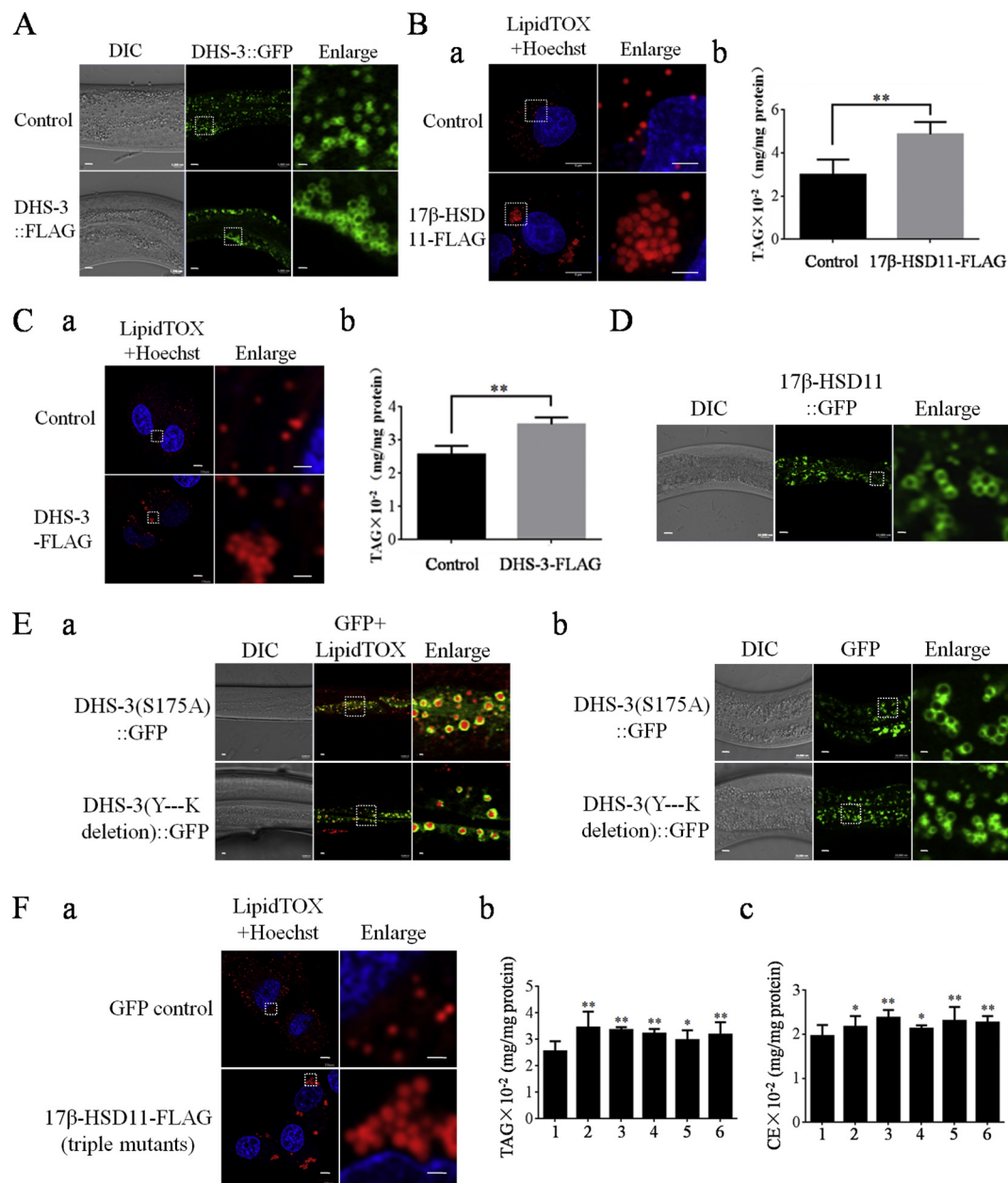
Fig. 4. Overexpression of DHS-3 and 17β-HSD11 induced LD aggregation and TAG accumulation. Catalytic site mutants also induced these phenotypes.
(A) *vha-6p::dhs-3::gfp* and *vha-6p::dhs-3::gfp; dhs-3p::dhs-3::flag* (a) animals were generated and visualized by confocal microscopy. Scale bar, 5 μm. Enlarged images: scale bar, 1 μm. (B) (a) GFP control and 17β-HSD11-FLAG were transfected into HeLa cells which were stained with LipidTOX red and were visualized by confocal microscopy. Scale bar, 5 μm. Enlarged images: scale bar, 1 μm. (b) TAG content normalized to total protein was quantified. Data are presented as mean ± SEM., n = 3. **P < 0.01, Two-way ANOVA. (C) (a) GFP control and DHS-3-FLAG were transfected into HeLa cells which were stained with Hoechst and LipidTOX red and were visualized by confocal microscopy. Scale bar, 5 μm. Enlarged images: scale bar, 1 μm. (b) TAG content normalized to total protein was quantified. Data presented as mean ± SEM., n = 3. **P < 0.05, two-tailed *t*-test. (D) *vha-6p::17-HSD11::gfp* transgenic animals were constructed and examined by confocal microscopy. Scale bar, 10 μm. Enlarged images: scale bar, 1 μm. (E) Transgenic animals with *dhs-3p*::DHS-3 (S175A)::GFP and *dhs-3p*::DHS-3 (Y—K188–192 deletion)::GFP were constructed and visualized by confocal microscopy (b). LDs were stained with LipidTOX red (a). Scale bar, 5 μm. Enlarged images: scale bar, 1 μm. (F) GFP control (1), 17β-HSD11-FLAG (2), 17β-HSD11 (GHGIG45-49AAAAA)-FLAG (3), 17β-HSD11 (S172A)-FLAG (4), 17β-HSD11 (YCSSK185-189AAAAA)-FLAG (5), and 17β-HSD11 (triple mutants) (6) were transfected in HeLa cells. TAG (b) and CE (c) content normalized to total protein was quantified. Data presented as mean ± SEM., n = 3. **P < 0.05, two-tailed t-test. GFP control and 17β-HSD11-FLAG (triple mutants)-overexpressing cells were examined by confocal microscopy with LipidTOX staining (a). Scale bar, 5 μm. Enlarged images: scale bar, 1 μm.

level of DHS-3 in various strains could affect LD distribution. To further explore this possibility, *dhs-3p*::DHS-3::Flag was exogenously expressed in the *dhs-3* single copy transgenic worm (Fig. S5a), resulting in strongly clustered LDs (Fig. 4A).

Based on this finding, we investigated whether 17β-HSD11 would induce a similar phenotype in mammalian cells. Expression of 17β-HSD11::FLAG was expressed in HeLa cells (Fig. S5b) induced LD

clustering, in contrast to control cells that expressed GFP (Fig. 4Ba). In addition, TAG assay showed there was a notable increase in TAG content in 17β-HSD11::FLAG-overexpressing cells (Fig. 4Bb).

We next tested whether these proteins had evolutionarily conserved ability to induce LD clustering. DHS-3::FLAG was overexpressed in in HeLa cells, which resulted in clear LD clustering and elevated TAG content (Fig. 4C, Fig. S5c). Similarly, 17β-HSD11::GFP induced LD
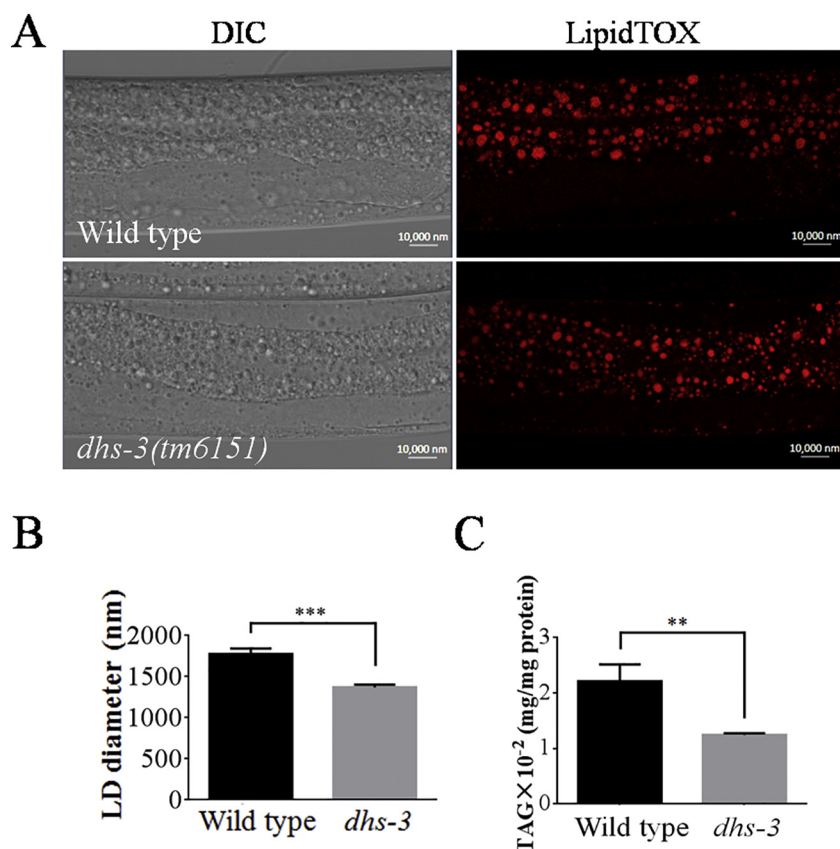
Fig. 5. DHS-3 knock out caused a decrease in LD size and TAG content.
(A) L4 worms of wild type and *dhs-3* mutants were fixed and stained with LipidTOX. Scale bar, 5 μm. (b) The diameters of stained LDs were quantified. Data represent mean ± SEM. n = 20. ***P < 0.0001, two-tailed t-test. (c) TAG content normalized to total protein was quantified. Data presented as mean ± SEM., n = 3. **P < 0.05, two-tailed t-test.

aggregation in *C. elegans* (Fig. 4D). Collectively, these results reveal that DHS-3 and 17β-HSD11 regulate LD dynamics with similar mechanisms in diverse eukaryotic models.

3.8. The catalytic sites of the 17β-HSDs are not involved in their localization or influence on LD clustering

The 17β-HSDs belong to the SDR family of enzymes that contain a variable N-terminal Gly-X3-Gly-X-Gly motif as part of the NAD (P) binding region and a substrate binding region formed by a catalytic triad of Ser (S), Tyr (Y), and Lys (K) residues [77]. The sequence alignment of DHS-3 and 17β-HSD11 showed that these two proteins possessed the common Gly-rich motif and active site (Fig. 1A). Therefore, catalytic site mutants of these 17β-HSDs were created and expressed to determine whether enzymatic activity was involved in their localization and function.

Both DHS-3 (S175A)::GFP and DHS-3 (Y—K188–192 deletion)::GFP were found to clearly surround LDs when expressed in *C. elegans* (Fig. 4Ea). Interestingly, both DHS-3 (S175A)::GFP and DHS-3 (Y—K188–192 deletion)::GFP also induced LD clustering in *C. elegans* similar to that seen with wild type DHS-3::GFP overexpressed worms (Fig. 4Eb). Similarly, overexpression of 17β-HSD11 (G-G-G45-49AAAAA)-FLAG, 17β-HSD11 (S172A)-FLAG, 17β-HSD11 (Y—K185-189AAAAA)-FLAG, and 17β-HSD11 (triple mutants)-FLAG in HeLa cells resulted in increased TAG and CE content (Fig. 4Fb, Fc, Fig. S5d). Furthermore, overexpression of 17β-HSD11 (triple mutants)- FLAG was observed to induce clustered LDs (Fig. 4Fa). Other enzymatic site mutants produced a similar LD aggregation phenotype (data not shown). Collectively, these results clearly demonstrate that the catalytic sites of the 17β-HSDs do not participate in their localization or their regulation of LDs clustering.

3.9. There is no evidence of ro01416 involvement in the regulation of LD distribution and size in RHA1

We next investigated the ability of ro01416 to influence LD clustering and size in RHA1. Ro01416-GFP was expressed in RHA1 and the cells were stained with LipidTOX red. The cells were examined by confocal microscopy and the fluorescence images showed no apparent differences between wild type and the transfected cells (Fig. S6a). Similar to DHS-3 and 17β-HSD11, ro01416 possesses the common Gly-rich motif and active site. We expressed ro01416 (S144 deletion)-GFP and ro01416 (Y—K157–161 deletion)-GFP in RHA1 and processed the cells for imaging. Both deletion mutants were targeted to LDs and the LD distribution and size were unchanged from that of the wild type cells (Fig. S6b). Biochemical analysis confirmed that these two GFP tagged catalytic site mutants were targeted to LDs (Fig. S6c).

Next, we constructed a ro01416-KO (knock out) strain which was confirmed by PCR (Fig. S6d, Fig. S6e). There was no change in the size or distribution of LDs in the knockout cells (Fig. S6f). Furthermore, there were no differences in the amount of TAG in ro01416-KO, ro01416-KO-ro01416-GFP, ro01416-GFP, ro01416-KO-ro01416 (S144 deletion)-GFP or ro01416-KO-ro01416 (Y—K157–161 deletion)-GFP strains (Fig. S6 g). Therefore, the ro01416 protein does not appear to have any influence on the regulation of LD distribution and size.

3.10. Loss of function of DHS-3 down regulates fat storage

As DHS-3 and 17β-HSD11 have been determined to induce LD aggregation, we undertook a functional study using deletions mutants. We leveraged the genetic tractability of *C. elegans* to examine the phenotype of *dhs-3* mutants. Previous studies showed a clear decrease in LD size in *dhs-3 (gk873395)* mutants [75]. For our study we examined *dhs-3 (tm6151)* which deleted 547 bp stretching from the promoter region to the second exon (Fig. S7a). The patterns of LD-associated proteins
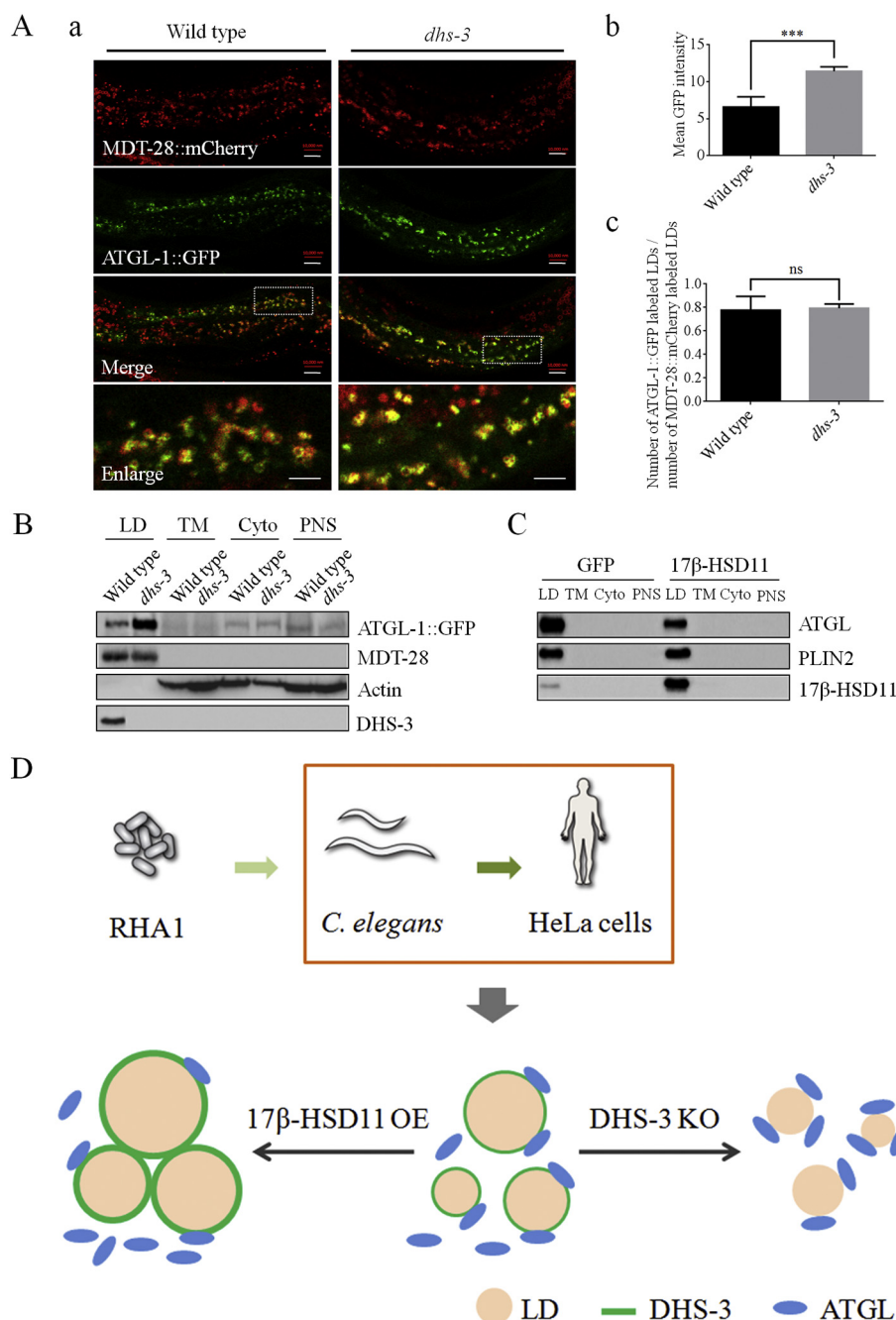
Fig. 6. DHS-3 and 17β-HSD11 affected the localization of ATGL on LDs.

(A) (a) *mdt-28/plin-1p::mdt-28/plin-1::mCherry; vha-6p::atgl-1::gfp* and *dhs-3; mdt-28/plin-1p::mdt-28/plin-1::mCherry; vha-6p::atgl-1::gfp* animals were visualized by confocal microscopy. Scale bar, 10 μm. Enlarged images: scale bar, 5 μm. (b) Quantification of ATGL-1::GFP fluorescence intensity in (a). Data represent mean ± s.d., n = 5. ***P < 0.0001, two-tailed t-test. (c) The percentage of ATGL-1::GFP and MDT-28/PLIN-1::mCherry colocalization was quantified. Data represent mean ± s.d., n = 5. ns, no significance. (B) Western blotting analysis showing increased ATGL-1 targeting to LDs in *dhs-3* mutants. *vha-6p::atgl-1::gfp* and *dhs-3; vha-6p::atgl-1::gfp* animals were collected and fractionated. The fractions were analyzed by Western blotting, probing with anti-GFP. MDT-28/PLIN-1, Actin and DHS-3 were probed as controls. (C) Western blotting analysis showing decreased ATGL targeting to LDs in 17β-HSD11-overexpressing HeLa cells. GFP control and 17β-HSD11-overexpressing cells were collected and fractionated. The distribution of endogenous ATGL in different fractions was analyzed by Western blotting with anti-ATGL. PLIN2 and 17β-HSD11 were detected as controls. (D) The model of DHS-3 and 17β-HSD11 regulating LD size and distribution and affecting the localization of ATGL on LDs. In *C. elegans*, *dhs-3* knockout (KO) caused small LDs and increased ATGL-1 protein on LDs. In HeLa cells, overexpression (OE) of 17β-HSD11 induced LD clustering and decreased ATGL protein on LDs.

from the mutants and wild type animals were compared by silver staining and Western blotting. A 36 kDa band present in the wild type LD protein extract was absent in the *dhs-3* deletion mutants. Western blotting confirmed knockout of DHS-3 in the mutants (Fig. S7b, Fig. S7c).

To examine the effects of DHS-3 knockout on LD distribution and size, *dhs-3* mutants and wild type animals were fixed with paraformaldehyde and stained by LipidTOX red. The fluorescence images were used to quantify LD size. The LDs in *dhs-3* mutants were significantly smaller than those in wild type animals (Fig. 5A, B). In addition, there was an obvious reduction of TAG content in *dhs-3* mutants (Fig. 5C). LDs were purified from *dhs-3* mutants and wild type animals which were then stained by LipidTOX red. The size of LDs from *dhs-3* mutants was decreased compared with wild type (Fig. S8a). The size of the isolated LDs was measured by a Delsa Nano C particle analyzer. By this analysis the mean LD diameter of *dhs-3* mutants was smaller than

that of wild type (Fig. S8b). The results were consistent with our previous work in *dhs-3 (gk873395)* mutants [75].

3.11. DHS-3 regulation of fat storage is not dependent on SBP-1 or SCDs

Next we investigated whether DHS-3 influenced lipid storage through lipogenesis or lipolysis pathways. First, the lipogenesis pathway was investigated. SBP-1, the *C. elegans* SREBP1c ortholog, is required for efficient transcription of genes involved in fatty acid synthesis. Depletion of *sbp-1* resulted in significantly decreased fat stores [78]. Therefore, the double knockout strain *dhs-3; sbp-1* was created and the size of LDs was quantified. The double mutants had smaller LDs than either single mutant (Fig. S9a, Fig. S9b). There was no difference in SBP-1 mRNA level in the *dhs-3* mutants (Fig. S9e). There was no apparent change in nuclear localization of GFP::SBP-1 in animals treated with *dhs-3* RNAi (Fig. S9f). Together, these results suggest

that DHS-3 influences lipid storage by a pathway independent of SBP-1.

Three genes, *fat-5*, *fat-6* and *fat-7*, encode stearoyl-CoA desaturases (SCDs) in *C. elegans* and these proteins operate downstream of *sbp-1*. It is known that *fat-6; fat-7* double mutants accumulate less fat than wild type [79]. Therefore, we generated a *dhs-3; fat-6; fat-7* triple mutants. The triple mutants had smaller LDs than the *fat-6; fat-7* double mutants (Fig. S9c, Fig. S9d), suggesting that DHS-3 also does not function in the same pathway as FAT-6 and FAT-7.

3.12. Inactivation of dhs-3 results in small LDs dependent on atgl-1

Since *dhs-3* deletion reduced fat storage in the lipid synthesis defective mutants, we suspected that *dhs-3* deletion resulted in accelerated lipolysis. Adipose triglyceride lipase (ATGL) is the rate-limiting enzyme for triglyceride catabolism in mammals and *C. elegans* [80,81]. The ATGL ortholog in *C. elegans* is encoded by *atgl-1*. Therefore, we knocked down *atgl-1* by RNAi in wild type and *dhs-3* mutants and quantified LD size by LipidTOX red staining. The RNAi resulted in increased LD size in wild type and significantly restored LD size in the *dhs-3* mutants (Fig. S10a, Fig. S10b). Next, *sbp-1* mutants and *dhs-3; sbp-1* double mutants were treated with *atgl-1* RNAi. Knockdown of *atgl-1* had no effect on LD size in *sbp-1* mutants. However, *atgl-1* RNAi significantly increased LD size in *dhs-3; sbp-1* double mutants (Fig. S10c, Fig. S10d). Together, the data suggest that *atgl-1* is involved in the accelerating lipid metabolism in *dhs-3* inactive worms.

3.13. DHS-3 and 17β-HSD11 affect the localization of ATGL on LDs

The mechanism by which ATGL-1 affected lipid storage in *dhs-3* mutants was investigated. First, ATGL-1 mRNA level was measured by RT-PCR to determine if *dhs-3* knockout influenced it. However, the knockout had no effect on ATGL-1 mRNA level (Fig. S11a). Next, transgenic ATGL-1::GFP animals were generated in *dhs-3* mutants to determine if the ATLG-1 protein level was altered by *dhs-3* knockout. Fluorescence micrographs showed no clear change in ATGL::GFP protein levels between wild type and *dhs-3* mutants (Fig. S11b). Furthermore, quantification of GFP showed no obvious change in *dhs-3* mutants (Fig. S11c). However, Western blotting of ATGL-1::GFP exhibited a slightly increase signal in *dhs-3* mutants (Fig. S11d).

The localization of ATGL-1::GFP was investigated. Fluorescence micrographs showed that the GFP fluorescence on separate LD labeled by MDT-28/PLIN-1::mCherry increased in *dhs-3* mutants (Fig. 6Aa, Ab), but the percentage of ATGL-1::GFP and MDT-28/PLIN-1::mCherry co-localization in *dhs-3* mutants has no significant change (Fig. 6Ac). Moreover, it was found that loss function of DHS-3 led to a significant increase of ATGL-1 on LDs by Western blotting (Fig. 6B). Thus, a loss of DHS-3 promotes ATGL-1 translocation to LDs.

Overexpression of 17βHSD11, the ortholog of DHS-3 in mammals, caused LD aggregation similar to that of DHS-3. Thus, we investigated whether 17β-HSD11 could affect the localization of ATGL on LDs. Control and 17β-HSD11-overexpressing HeLa cells were fractionated by differential centrifugation and the fractions were analyzed by Western blotting. Exogenous expression of 17β-HSD11 resulted in a reduction of ATGL on LDs without changing the localization or abundance of PLIN2 (Fig. 6C). Together, these results reveal that DHS-3 and 17β-HSD11 regulate LD size and distribution in a similar manner, possibly through the modulation of ATGL recruitment to LDs (Fig. 6D).

3.14. Loss of function of DHS-3 affects the progeny and growth rates of worms with a defect in fat synthesis

DHS-3 and 17β-HSD11 clearly have significant influence on LD size, LD distribution and lipid metabolism. We were interested in determining what larger physiological roles these proteins play at the organismal level. *C. elegans* is a good model for physiological function studies. Therefore, lifespan, L1 survival, hatch rate, progeny and

growth rate of *dhs-3* mutants were assessed. However, there were no significant changes compared with wild type (data not shown). It has been reported that *sbp-1* mutants generated fewer progeny and displayed growth defects [78]. We found that *dhs-3; sbp-1* double mutants produced fewer progeny and had slower growth than the single mutants (Fig. S12a, Fig. S12b). In addition, loss function of DHS-3 further reduced progeny production and slowed the growth of *fat-6; fat-7* double mutants (Fig. S12c, Fig. S12d). Therefore, DHS-3 impacts progeny and growth rate in worms containing a defect in fat synthesis.

4. Discussion

4.1. HSDs localize on LDs in different organisms, different tissues and cell types, as well as LDs in cytosol and nucleus, and different cytoplasmic LD subsets

In our study, we have summarized the majority of available LD proteomic data. Several SDRs and a subset of HSDs, the 3β-HSDs, 11β-HSDs and 17β-HSDs, have been broadly identified on LDs across tissues and organisms, suggesting an ancient role for this family in lipid metabolism. To analyze the relationships among the HSD proteins, datasets from 12 organisms covering 37 proteins were summarized (Table S5). Using this dataset, the Maximum Likelihood tree for orthologous and paralogous proteins of the HSD family was generated (Fig. S13). It can be inferred from the tree that HSD proteins have been subjected to substantial selective pressure resulting in repeated loss and gain of function mutations. Multiple duplication events and higher level mutations have resulted in a large protein family with members performing diverse functional roles across organisms, tissues, and organelles.

The involvement of HSD family in LD function can be traced back to bacteria, demonstrating the ancient origins of this role. In this study, the HSD protein, ro01416, was identified on LDs in RHA1. The protein ENV9, an ortholog of RDH12 in humans, targeted to LDs in *S. cerevisiae* [82]. DHS-3 and its paralogs were targeted to LDs in *C. elegans*, CG2254 was found on LDs in *Drosophila* [21,83], and 17β-HSD11 and 17β-HSD13 were localized on mammalian LDs [12,71]. However, as the available phylogenetic tree is incomplete, it is not possible to draw firm conclusions on the evolutionary relationships among the LD-targeted HSDs.

An evolutionary expansion of the HSD family accompanied increased cellular complexity. The development of organelles and multicellularity saw increased complexity in expression patterns of the growing protein family (Fig. 2H). A given LD may have multiple HSDs and some HSDs can be found in several different tissues. In *C. elegans*, we found DHS-3, DHS-4 and DHS-19 on LDs in different tissues. DHS-3 was expressed in the intestine, the main lipid storage site. DHS-4 was expressed in hypodermis, and DHS-19 was in the hypodermis and possibly localized on LDs in the muscle. In humans, 17β-HSD11 was targeted to LDs in epithelium, skeletal muscle, liver, intestine and other tissues. However, 17β-HSD13, which was very similar to 17β-HSD11, exhibited liver-specific expression [42]. The other 17β-HSDs (labeled by purple in Fig. 2H) were reported to be expressed in several tissues [84–90]. In the summary of LD proteomes, 17β-HSD2, 17β-HSD4, 17β-HSD7 and 17β-HSD12 were present on LDs in several tissues. In contrast, 17β-HSD6 was present only on liver LDs, and 17β-HSD8 and 17β-HSD10 were found only in BAT LDs of mice.

In addition to the differential expression of these proteins across tissue types, these proteins also vary in their intracellular localization (Fig. 2H). In eukaryotic cells, neutral lipids are mainly stored in cytoplasmic LDs. Recently nuclear LDs were also found in hepatic tissues and liver cells [76,91,92]. Here, DHS-9::GFP was shown to partially localize on both cytoplasmic and nuclear LDs in *C. elegans*. And it was predominantly on nuclear LDs in the intestinal cells with only a weak cytoplasmic signal. However, besides the colocalization of MDT-28/PLIN-1::mCherry::NLS and DHS-9::GFP in the nuclear, it will require

more sensitive tests to demonstrate that DHS-9::GFP label nuclear LDs in *C. elegans* in the future. Following OA treatment, DHS-9 was partially targeted to both cytoplasmic LDs and nuclear LDs in Huh7 cells, so the nuclear localization of the GFP-tagged protein may be physiologic. In humans, DHRS1, the DHS-9 ortholog, could also localize on cytoplasmic and nuclear LDs. In our phylogenetic analysis, the DHRS1 family had a distant relationship with the other HSD proteins. Other HSDs are mainly localized on cytoplasmic LDs. For example, DHS-3 is absent from the nucleus. It is clear that DHRS1 family members can be targeted to both cytoplasmic and nuclear LDs, and it may be that the nuclear-targeted proteins have distinct nuclear localization signals (Fig. 2H).

In the cytosol, proteins are targeted to different subsets of LDs by an unknown mechanism. For example, in *Drosophila*, CG2254 was recently found on different LD subsets as mediated by two distinct targeting motifs [83]. Together, HSDs could localize on LDs in different organisms, tissues and cell types, cytoplasmic and nuclear LDs, as well as different cytoplasmic LDs (Fig. 2H). However, their mechanisms and functional significance of these differing localizations are not clear.

4.2. LD targeting of 17β-HSD proteins

In our study, we found that the related proteins DHS-3 and 17β-HSD11 were major LD proteins in *C. elegans* and humans, respectively. It seems that 17β-HSDs do not form continuous rings in *C. elegans*, but are present only on part of the LD periphery in Fig. 3A. This is a common phenomenon. When fixation and staining are used to visualize LDs for certain dyes, LD-associated proteins are disturbed dramatically. In Fig. 4D, it can be seen that 17β-HSDs form continuous ring on individual LD in *C. elegans* without fixation.

DHS-3 and 17β-HSD11 targeted to LDs by an N-terminal hydrophobic domain and could be appropriately targeted to LDs in diverse eukaryotic organisms. However, neither was targeted to LDs when expressed in RHA1, with the proteins showing only a diffuse cytoplasmic distribution. Similarly, ro01416-GFP was found on LDs in RHA1 but gave only a diffuse cytoplasmic distribution when expressed in *C. elegans* or HeLa cells (data not shown). It is suspected that the eukaryotic proteins are not folded properly when expressed in bacteria and *vice versa*. It is also possible that differences in LD membrane composition prevent appropriate targeting. Eukaryotic membranes are rich in phosphatidylcholine (PC) while prokaryotic membranes are rich in phosphatidylethanolamine (PE) [93,94]. Our finding suggests that ro01416 targets to adiposomes inefficiently compared with the other proteins may be due to the adiposomes construction with PC.

It is known that the hydrophobic N-termini of DHS-3 and 17β-HSD11 and the hydrophobic C-terminus of ro01416 are required for LD targeting. However, no more details are known and there is no known common targeting motif across HSD family proteins. It has been reported that the sequence adjacent to the N-terminal hydrophobic domain in 17β-HSD11 had a weak homology with the PAT motif. And both of them are sufficient for ER localization with LDs and LD localization of 17β-HSD11 [95]. Thus, it remains unknown if LD targeted proteins like the HSDs, the PAT family, and APO-like proteins share a common targeting mechanism [96].

4.3. 17β-HSD11 family proteins regulate LD distribution and size in C. elegans and human cells

Overexpression of DHS-3 and 17β-HSD11 was found to cause LD aggregation in *C. elegans* and HeLa cells. It is similar to that overexpression of AUP1 induces LD clustering in COS7 cells. The CUE domain of AUP1, the ubiquitin-binding domain, is not involved in LD localization of AUP1, but is important for LD clustering [97]. Whereas the protein enzymatic sites of DHS-3 and 17β-HSD11 were not involved in the LD targeting or in the LD aggregation, which suggests that these two proteins promote LD distribution with a different underlying mechanism. This was consistent with the previous finding that the

enzymatic activity of CG2254 is not a strict requirement for its LD subset location [83]. In contrast, it has been reported that overexpression of Env9 led to the formation of fewer, larger LDs and that Env9 oxidoreductase activity was essential for this effect [82], which highlights the diversity and complexity of SDRs on LDs. Overexpression of DHS-3 and 17β-HSD11 also induced TAG accumulation in HeLa cells but not in *C. elegans*, suggesting other HSDs may serve to regulate TAG accumulation in *C. elegans*.

In other experiments, a reduction in LD-associated ATGL was seen in 17β-HSD11-overexpressing cells. Knock out of DHS-3 resulted in small LDs, decreased TAG, and increased ATGL on LDs. These results indicate that DHS-3 and 17β-HSD11 may affect lipid through the regulation of lipolysis. The increased lipolysis in *dhs-3* mutants affected the lipid content, brood size, and growth rate in worms that are defective in lipogenesis. The SDRs were known to function as dimmers and tetramers [77]. Therefore, DHS-3 and 17β-HSD11 may form oligomers which form a protective layer on LDs, and the possible interaction between the proteins on different LDs may promote LD aggregation. However, further work is needed to elucidate the detailed mechanisms by which LD-localized HSDs influence LD size, distribution and function. And whether DHS-3 and 17β-HSD11 function as enzymes in other cellular processes and the functional significance of LD localization for the other HSD proteins remain unknown.

Both of *dhs-3 (tm6151)* and *dhs-3 (gk873395)* were separately back-crossed for 6 times, and small LDs were observed in these two alleles. Besides, the *dhs-3* RNAi showed decreased LD size. Further, like the phenotypes in *dhs-3; sbp-1* mutants, *dhs-3* RNAi also enhanced the defect of lipid, brood size and growth rate in *sbp-1* mutants (data not shown). These results verified that loss of *dhs-3* caused small LDs. In the rescue of small LDs in *dhs-3 (tm6151)* mutants, the expression of DHS-3 (isoform a)::GFP, fosmid containing *dhs-3* gene, and *dhs-3* genomic DNA (extrachromasomal arrays) showed no rescue. The single copy *hjSi224* also cannot rescue (data not shown). We suspect that the expression level of DHS-3 is not well control although the single copy is already low expressed. It needs further investigation.

4.4. Ro01416 has no significant role in LD regulation

Ro01416, an ortholog of human 17β-HSD12, was identified on LDs in RHA1. Overexpression of ro01416-GFP had no significant effects on LD size or distribution. Also, LD size and TAG content were unchanged in ro01416 knock out cells. The possible reasons may include the following: 1) LD dynamics is difficult to observe in RHA1 due to their small size; 2) ro01416, although targeted to LDs, has a distinct function from its presumed orthologs, not impacting LD dynamics. It may be that ro01416 is one of a set of LD-associated HSDs which are not major LD proteins, unlike DHS-3 and 17β-HSD11. It may be that LD targeting of HSDs in ancient cell types serves other functions like signaling while having no roles in regulation of LD size or lipid storage. Perhaps the other roles of this class of protein evolved over time with the increased complexity of the cells and the functions of LDs.

4.5. These findings contribute to LD studies

From prokaryotes to mammals, a large number of HSDs have been identified to localize on LDs. These proteins serve not only as excellent LD markers but also provide a new perspective on the study of LD evolution and diversity. These enzymes will likely be found to have important roles in lipid metabolism and LD regulation.

Transparency document

The http://dx.doi.org/10.1016/j.bbalip.2018.04.018 associated with this article can be found, in online version.

Acknowledgments

Author contributions

P.L. conceived the project. Y.L., S.X. and C.Z. carried out experiments and data analysis. Y.L. performed experiments in *C. elegans* and *in vitro*, S.X. performed experiments in HeLa cells and C.Z. performed experiments in RHA1. X.Z. performed the LD proteome summary. M.H. performed the homolog summary and conducted the phylogenetic analyses. M.C. contributed to critical reading and useful suggestions. Experiments and manuscript were assisted by contributions from X.Z. and H.Z. Manuscript was written by Y.L. and P.L.

Competing interests

The authors declare no competing financial interests.

Appendix A. Supplementary data

Supplementary data to this article can be found online at https://doi.org/10.1016/j.bbalip.2018.04.018.

References

[1] B. Sanjabi, M. Dashty, B. Ozcan, V. Akbarkhanzadeh, M. Rahimi, M. Vinciguerra, F. van Rooij, S. Al-Lahham, F. Sheedfar, T.G. van Kooten, et al., Lipid droplets hypertrophy: a crucial determining factor in insulin regulation by adipocytes, Sci. Rep. 5 (2015) 8816.

[2] D.G. Mashek, S.A. Khan, A. Sathyanarayan, J.M. Ploeger, M.P. Franklin, Hepatic lipid droplet biology: getting to the root of fatty liver, Hepatology 62 (2015) 964–967.

[3] A.S. Greenberg, R.A. Coleman, F.B. Kraemer, J.L. McManaman, M.S. Obin, V. Puri, Q.W. Yan, H. Miyoshi, D.G. Mashek, The role of lipid droplets in metabolic disease in rodents and humans, J. Clin. Invest. 121 (2011) 2102–2110.

[4] Y. Chen, Y. Ding, L. Yang, J. Yu, G. Liu, X. Wang, S. Zhang, D. Yu, L. Song, H. Zhang, et al., Integrated omics study delineates the dynamics of lipid droplets in Rhodococcus opacus PD630, Nucleic Acids Res. 42 (2014) 1052–1064.

[5] Y. Ding, L. Yang, S. Zhang, Y. Wang, Y. Du, J. Pu, G. Peng, Y. Chen, H. Zhang, J. Yu, et al., Identification of the major functional proteins of prokaryotic lipid droplets, J. Lipid Res. 53 (2012) 399–411.

[6] C. Zhang, P. Liu, The lipid droplet: a conserved cellular organelle, Protein Cell 8 (11) (2017) 796–800.

[7] A.R. Thiam, M. Beller, The why, when and how of lipid droplet diversity, J. Cell Sci. 130 (2017) 315–324.

[8] T. Fujimoto, R.G. Parton, Not just fat: the structure and function of the lipid droplet, Cold Spring Harb. Perspect. Biol. 3 (2011).

[9] P. Liu, Y. Ying, Y. Zhao, D.I. Mundy, M. Zhu, R.G. Anderson, Chinese hamster ovary K2 cell lipid droplets appear to be metabolic organelles involved in membrane traffic, J. Biol. Chem. 279 (2004) 3787–3792.

[10] H. Zhang, Y. Wang, J. Li, J. Yu, J. Pu, L. Li, H. Zhang, S. Zhang, G. Peng, F. Yang, et al., Proteome of skeletal muscle lipid droplet reveals association with mitochondria and apolipoprotein a-I, J. Proteome Res. 10 (2011) 4757–4768.

[11] P. Zhang, H. Na, Z. Liu, S. Zhang, P. Xue, Y. Chen, J. Pu, G. Peng, X. Huang, F. Yang, et al., Proteomic study and marker protein identification of Caenorhabditis elegans lipid droplets, Mol. Cell. Proteomics 11 (2012) 317–328.

[12] W. Su, Y. Wang, X. Jia, W. Wu, L. Li, X. Tian, S. Li, C. Wang, H. Xu, J. Cao, et al., Comparative proteomic study reveals 17beta-HSD13 as a pathogenic protein in nonalcoholic fatty liver disease, Proc. Natl. Acad. Sci. U. S. A. 111 (2014) 11437–11442.

[13] M. Fukushima, M. Enjoji, M. Kohjima, S. Sugimoto, S. Ohta, K. Kotoh,

[14] M. Kuniyoshi, K. Kobayashi, M. Imamura, T. Inoguchi, et al., Adipose differentiation related protein induces lipid accumulation and lipid droplet formation in hepatic stellate cells, In Vitro Cell. Dev. Biol. Anim. 41 (2005) 321–324.

[14] K.M. Szymanski, D. Binns, R. Bartz, N.V. Grishin, W.P. Li, A.K. Agarwal, A. Garg, R.G. Anderson, J.M. Goodman, The lipodystrophy protein seipin is found at endoplasmic reticulum lipid droplet junctions and is important for droplet morphology, Proc. Natl. Acad. Sci. U. S. A. 104 (2007) 20890–20895.

[15] H. Jiang, J. He, S. Pu, C. Tang, G. Xu, Heat shock protein 70 is translocated to lipid droplets in rat adipocytes upon heat stimulation, Biochim. Biophys. Acta 1771 (2007) 66–74.

[16] J. McLauchlan, Lipid droplets and hepatitis C virus infection, Biochim. Biophys. Acta 1791 (2009) 552–559.

[17] A.R. Kimmel, C. Sztalryd, The perilipins: major cytosolic lipid droplet-associated proteins and their roles in cellular lipid storage, mobilization, and systemic homeostasis, Annu. Rev. Nutr. 36 (2016) 471–509.

[18] M.B. Trevino, Y. Machida, D.R. Hallinger, E. Garcia, A. Christensen, S. Dutta, D.A. Peake, Y. Ikeda, Y. Imai, Perilipin 5 regulates islet lipid metabolism and insulin secretion in a cAMP-dependent manner: implication of its role in the postprandial insulin secretion, Diabetes 64 (2015) 1299–1310.

[19] P.E. Bickel, J.T. Tansey, M.A. Welte, PAT proteins, an ancient family of lipid droplet proteins that regulate cellular lipid stores, Biochim. Biophys. Acta 1791 (2009) 419–440.

[20] S. Miura, J.W. Gan, J. Brzostowski, M.J. Parisi, C.J. Schultz, C. Londos, B. Oliver, A.R. Kimmel, Functional conservation for lipid storage droplet association among Perilipin, ADRP, and TIP47 (PAT)-related proteins in mammals, Drosophila, and Dictyostelium, J. Biol. Chem. 277 (2002) 32253–32257.

[21] M. Beller, D. Riedel, L. Jansch, G. Dieterich, J. Wehland, H. Jackle, R.P. Kuhnlein, Characterization of the Drosophila lipid droplet subproteome, Mol. Cell. Proteomics 5 (2006) 1082–1094.

[22] C. Schmidt, B. Ploier, B. Koch, G. Daum, Analysis of yeast lipid droplet proteome and lipidome, Methods Cell Biol. 116 (2013) 15–37.

[23] B. Persson, Y. Kallberg, J.E. Bray, E. Bruford, S.L. Dellaporta, A.D. Favia, R.G. Duarte, H. Jornvall, K.L. Kavanagh, N. Kedishvili, et al., The SDR (short-chain dehydrogenase/reductase and related enzymes) nomenclature initiative, Chem. Biol. Interact. 178 (2009) 94–98.

[24] M. Kisiela, A. Skarka, B. Ebert, E. Maser, Hydroxysteroid dehydrogenases (HSDs) in bacteria: a bioinformatic perspective, J. Steroid Biochem. Mol. Biol. 129 (2012) 31–46.

[25] B. Persson, Y. Kallberg, Classification and nomenclature of the superfamily of short-chain dehydrogenases/reductases (SDRs), Chem. Biol. Interact. 202 (2013) 111–115.

[26] Y. Kallberg, U. Oppermann, H. Jornvall, B. Persson, Short-chain dehydrogenase/reductase (SDR) relationships: a large family with eight clusters common to human, animal, and plant genomes, Protein Sci. 11 (2002) 636–641.

[27] D.L. Brasaemle, T. Barber, N.E. Wolins, G. Serrero, E.J. Blanchette-Mackie, C. Londos, Adipose differentiation-related protein is an ubiquitously expressed lipid storage droplet-associated protein, J. Lipid Res. 38 (1997) 2249–2263.

[28] N.E. Wolins, D.L. Brasaemle, P.E. Bickel, A proposed model of fat packaging by exchangeable lipid droplet proteins, FEBS Lett. 580 (2006) 5484–5491.

[29] O.V. Belyaeva, N.Y. Kedishvili, Comparative genomic and phylogenetic analysis of short-chain dehydrogenases/reductases with dual retinol/sterol substrate specificity, Genomics 88 (2006) 820–830.

[30] R.K. Kam, W. Shi, S.O. Chan, Y. Chen, G. Xu, C.B. Lau, K.P. Fung, W.Y. Chan, H. Zhao, Dhrs3 protein attenuates retinoic acid signaling and is required for early embryonic patterning, J. Biol. Chem. 288 (2013) 31477–31487.

[31] C. Deisenroth, Y. Itahana, L. Tollini, A. Jin, Y. Zhang, p53-Inducible DHRS3 is an endoplasmic reticulum protein associated with lipid droplet accumulation, J. Biol. Chem. 286 (2011) 28343–28356.

[32] W. Jiang, J.L. Napoli, The retinol dehydrogenase Rdh10 localizes to lipid droplets during acyl ester biosynthesis, J. Biol. Chem. 288 (2013) 589–597.

[33] M. Meier, G. Moller, J. Adamski, Perspectives in understanding the role of human 17beta-hydroxysteroid dehydrogenases in health and disease, Ann. N. Y. Acad. Sci. 1155 (2009) 15–24.

[34] L.M. Kuervers, C.L. Jones, N.J. O'Neil, D.L. Baillie, The sterol modifying enzyme LET-767 is essential for growth, reproduction and development in Caenorhabditis elegans, Mol. Gen. Genet. MGG 270 (2003) 121–131.

[35] E.V. Entchev, D. Schwudke, V. Zagoriy, A. Matyash, A. Bogdanova, B. Habermann, L. Zhu, A. Shevchenko, T.V. Kurzchalia, LET-767 is required for the production of branched chain and long chain fatty acids in Caenorhabditis elegans, J. Biol. Chem. 283 (2008) 17550–17560.

[36] A.J. O'Sullivan, D.M. Hoffman, K.K. Ho, Estrogen, lipid oxidation, and body fat, N. Engl. J. Med. 333 (1995) 669–670.

[37] B.A. Gower, T.R. Nagy, M.L. Blaylock, C. Wang, L. Nyman, Estradiol may limit lipid oxidation via Cpt 1 expression and hormonal mechanisms, Obes. Res. 10 (2002) 167–172.

[38] L.C. Gormsen, C. Host, B.E. Hjerrild, S.B. Pedersen, S. Nielsen, J.S. Christiansen, C.H. Gravholt, Estradiol acutely inhibits whole body lipid oxidation and attenuates lipolysis in subcutaneous adipose tissue: a randomized, placebo-controlled study in postmenopausal women, Eur. J. Endocrinol. 167 (2012) 543–551.

[39] K. Wend, P. Wend, B.G. Drew, A.L. Hevener, G.A. Miranda-Carboni, S.A. Krum, ERalpha regulates lipid metabolism in bone through ATGL and perilipin, J. Cell. Biochem. 114 (2013) 1306–1314.

[40] A. Belkaid, R.J. Ouellette, M.E. Surette, 17beta-estradiol-induced ACSL4 protein expression promotes an invasive phenotype in estrogen receptor positive mammary carcinoma cells, Carcinogenesis 38 (2017) 402–410.

[41] J. Schweisgut, C. Schutt, S. Wust, A. Wietelmann, B. Ghesquiere, P. Carmeliet, S. Drose, K.S. Korach, T. Braun, T. Boettger, Sex-specific, reciprocal regulation of ERalpha and miR-22 controls muscle lipid metabolism in male mice, EMBO J. 36 (2017) 1199–1214.

[42] Y. Horiguchi, M. Araki, K. Motojima, 17beta-Hydroxysteroid dehydrogenase type

13 is a liver-specific lipid droplet-associated protein, Biochem. Biophys. Res. Commun. 370 (2008) 235–238.

[43] C. Zhang, L. Yang, Y. Ding, Y. Wang, L. Lan, Q. Ma, X. Chi, P. Wei, Y. Zhao, A. Steinbuchel, et al., Bacterial lipid droplets bind to DNA via an intermediary protein that enhances survival under stress, Nat. Commun. 8 (2017) 15979.

[44] G. Peng, L. Li, Y. Liu, J. Pu, S. Zhang, J. Yu, J. Zhao, P. Liu, Oleate blocks palmitate-induced abnormal lipid distribution, endoplasmic reticulum expansion and stress, and insulin resistance in skeletal muscle, Endocrinology 152 (2011) 2206–2218.

[45] X. Chen, S. Xu, S. Wei, Y. Deng, Y. Li, F. Yang, P. Liu, Comparative proteomic study of fatty acid-treated myoblasts reveals role of cox-2 in palmitate-induced insulin resistance, Sci. Rep. 6 (2016) 21454.

[46] Y. Wang, X.M. Zhou, X. Ma, Y. Du, L. Zheng, P. Liu, Construction of nanodroplet/adiposome and artificial lipid droplets, ACS Nano 10 (2016) 3312–3322.

[47] J. Bouchoux, F. Beilstein, T. Pauquai, I.C. Guerrera, D. Chateau, N. Ly, M. Alqub, C. Klein, J. Chambaz, M. Rousset, et al., The proteome of cytosolic lipid droplets isolated from differentiated Caco-2/TC7 enterocytes reveals cell-specific characteristics, Biol. Cell. 103 (2011) 499–517.

[48] F. Beilstein, J. Bouchoux, M. Rousset, S. Demignot, Proteomic analysis of lipid droplets from Caco-2/TC7 enterocytes identifies novel modulators of lipid secretion, PLoS One 8 (2013) e53017.

[49] T. Yamaguchi, N. Fujikawa, S. Nimura, Y. Tokuoka, S. Tsuda, T. Aiuchi, R. Kato, T. Obama, H. Itabe, Characterization of lipid droplets in steroidogenic MLTC-1 Leydig cells: protein profiles and the morphological change induced by hormone stimulation, Biochim. Biophys. Acta 1851 (2015) 1285–1295.

[50] L. Davidi, Y. Levin, S. Ben-Dor, U. Pick, Proteome analysis of cytoplasmatic and plastidic beta-carotene lipid droplets in Dunaliella bardawil, Plant Physiol. 167 (2015) 60–79.

[51] S. Turro, M. Ingelmo-Torres, J.M. Estanyol, F. Tebar, M.A. Fernandez, C.V. Albor, K. Gaus, T. Grewal, C. Enrich, A. Pol, Identification and characterization of associated with lipid droplet protein 1: a novel membrane-associated protein that resides on hepatic lipid droplets, Traffic 7 (2006) 1254–1269.

[52] S. Larsson, S. Resjo, M.F. Gomez, P. James, C. Holm, Characterization of the lipid droplet proteome of a clonal insulin-producing beta-cell line (INS-1 832/13), J. Proteome Res. 11 (2012) 1264–1273.

[53] J. Yu, S. Zhang, L. Cui, W. Wang, H. Na, X. Zhu, L. Li, G. Xu, F. Yang, M. Christian, et al., Lipid droplet remodeling and interaction with mitochondria in mouse brown adipose tissue during cold treatment, Biochim. Biophys. Acta 1853 (2015) 918–928.

[54] V. Katavic, G.K. Agrawal, M. Hajduch, S.L. Harris, J.J. Thelen, Protein and lipid composition analysis of oil bodies from two Brassica napus cultivars, Proteomics 6 (2006) 4586–4598.

[55] P. Jolivet, E. Roux, S. D'Andrea, M. Davanture, L. Negroni, M. Zivy, T. Chardot, Protein composition of oil bodies in Arabidopsis thaliana ecotype WS, Plant Physiol. Biochem. 42 (2004) 501–509.

[56] F. Capuano, N.J. Bond, L. Gatto, F. Beaudoin, J.A. Napier, E. Benvenuto, K.S. Lilley, S. Baschieri, LC-MS/MS methods for absolute quantification and identification of proteins associated with chimeric plant oil bodies, Anal. Chem. 83 (2011) 9267–9272.

[57] P. Jolivet, C. Boulard, A. Bellamy, C. Larre, M. Barre, H. Rogniaux, S. d'Andrea, T. Chardot, N. Nesi, Protein composition of oil bodies from mature Brassica napus seeds, Proteomics 9 (2009) 3268–3284.

[58] P. Jolivet, C. Boulard, A. Bellamy, B. Valot, S. d'Andrea, M. Zivy, N. Nesi, T. Chardot, Oil body proteins sequentially accumulate throughout seed development in Brassica napus, J. Plant Physiol. 168 (2011) 2015–2020.

[59] K. Athenstaedt, D. Zweytick, A. Jandrositz, S.D. Kohlwein, G. Daum, Identification and characterization of major lipid particle proteins of the yeast Saccharomyces cerevisiae, J. Bacteriol. 181 (1999) 6441–6448.

[60] D. Binns, T. Januszewski, Y. Chen, J. Hill, V.S. Markin, Y. Zhao, C. Gilpin, K.D. Chapman, R.G. Anderson, J.M. Goodman, An intimate collaboration between peroxisomes and lipid bodies, J. Cell Biol. 173 (2006) 719–731.

[61] V.A. Ivashov, K. Grillitsch, H. Koefeler, E. Leitner, D. Baeumlisberger, M. Karas, G. Daum, Lipidome and proteome of lipid droplets from the methylotrophic yeast Pichia pastoris, Biochim. Biophys. Acta 1831 (2013) 282–290.

[62] S. Sato, M. Fukasawa, Y. Yamakawa, T. Natsume, T. Suzuki, I. Shoji, H. Aizaki, T. Miyamura, M. Nishijima, Proteomic profiling of lipid droplet proteins in hepatoma cell lines expressing hepatitis C virus core protein, J. Biochem. 139 (2006) 921–930.

[63] Y. Ding, Y. Wu, R. Zeng, K. Liao, Proteomic profiling of lipid droplet-associated proteins in primary adipocytes of normal and obese mouse, Acta Biochim. Biophys. Sin. 44 (2012) 394–406.

[64] D.L. Brasaemle, G. Dolios, L. Shapiro, R. Wang, Proteomic analysis of proteins associated with lipid droplets of basal and lipolytically stimulated 3T3-L1 adipocytes, J. Biol. Chem. 279 (2004) 46835–46842.

[65] E. Umlauf, E. Csaszar, M. Moertelmaier, G.J. Schuetz, R.G. Parton, R. Prohaska, Association of stomatin with lipid bodies, J. Biol. Chem. 279 (2004) 23699–23709.

[66] H.C. Wan, R.C. Melo, Z. Jin, A.M. Dvorak, P.F. Weller, Roles and origins of leukocyte lipid bodies: proteomic and ultrastructural studies, FASEB J. 21 (2007) 167–178.

[67] K. Grillitsch, M. Connerth, H. Kofeler, T.N. Arrey, B. Rietschel, B. Wagner, M. Karas, G. Daum, Lipid particles/droplets of the yeast Saccharomyces cerevisiae revisited: lipidome meets proteome, Biochim. Biophys. Acta 1811 (2011) 1165–1176.

[68] K. Athenstaedt, P. Jolivet, C. Boulard, M. Zivy, L. Negroni, J.M. Nicaud, T. Chardot, Lipid particle composition of the yeast Yarrowia lipolytica depends on the carbon source, Proteomics 6 (2006) 1450–1459.

[69] S. Cermelli, Y. Guo, S.P. Gross, M.A. Welte, The lipid-droplet proteome reveals that droplets are a protein-storage depot, Curr. Biol. 16 (2006) 1783–1795.

[70] R. Bartz, J.K. Zehmer, M. Zhu, Y. Chen, G. Serrero, Y. Zhao, P. Liu, Dynamic activity of lipid droplets: protein phosphorylation and GTP-mediated protein translocation, J. Proteome Res. 6 (2007) 3256–3265.

[71] Y. Fujimoto, H. Itabe, J. Sakai, M. Makita, J. Noda, M. Mori, Y. Higashi, S. Kojima, T. Takano, Identification of major proteins in the lipid droplet-enriched fraction isolated from the human hepatocyte cell line HuH7, Biochim. Biophys. Acta (BBA) - Mol. Basis Dis. 1644 (2004) 47–59.

[72] T.O. Eichmann, L. Grumet, U. Taschler, J. Hartler, C. Heier, A. Woblistin, L. Pajed, M. Kollroser, G. Rechberger, G.G. Thallinger, et al., ATGL and CGI-58 are lipid droplet proteins of the hepatic stellate cell line HSC-T6, J. Lipid Res. 56 (2015) 1972–1984.

[73] H.A. Saka, J.W. Thompson, Y.S. Chen, L.G. Dubois, J.T. Haas, A. Moseley, R.H. Valdivia, Chlamydia trachomatis infection leads to defined alterations to the lipid droplet proteome in epithelial cells, PLoS One 10 (2015) e0124630.

[74] T.L. Vrablik, V.A. Petyuk, E.M. Larson, R.D. Smith, J.L. Watts, Lipidomic and proteomic analysis of Caenorhabditis elegans lipid droplets and identification of ACS-4 as a lipid droplet-associated protein, Biochim. Biophys. Acta 1851 (2015) 1337–1345.

[75] H. Na, P. Zhang, Y. Chen, X. Zhu, Y. Liu, Y. Liu, K. Xie, N. Xu, F. Yang, Y. Yu, et al., Identification of lipid droplet structure-like/resident proteins in Caenorhabditis elegans, Biochim. Biophys. Acta 1853 (2015) 2481–2491.

[76] Y. Ohsaki, T. Kawai, Y. Yoshikawa, J. Cheng, E. Jokitalo, T. Fujimoto, PML isoform II plays a critical role in nuclear lipid droplet formation, J. Cell Biol. 212 (2016) 29–38.

[77] C. Filling, K.D. Berndt, J. Benach, S. Knapp, T. Prozorovski, E. Nordling, R. Ladenstein, H. Jornvall, U. Oppermann, Critical residues for structure and catalysis in short-chain dehydrogenases/reductases, J. Biol. Chem. 277 (2002) 25677–25684.

[78] B. Liang, K. Ferguson, L. Kadyk, J.L. Watts, The role of nuclear receptor NHR-64 in fat storage regulation in Caenorhabditis elegans, PLoS One 5 (2010) e9869.

[79] T.J. Brock, J. Browse, J.L. Watts, Fatty acid desaturation and the regulation of adiposity in Caenorhabditis elegans, Genetics 176 (2007) 865–875.

[80] C.C. Lord, J.M. Brown, Distinct roles for alpha-beta hydrolase domain 5 (ABHD5/CGI-58) and adipose triglyceride lipase (ATGL/PNPLA2) in lipid metabolism and signaling, Adipocytes 1 (2012) 123–131.

[81] J.H. Lee, J. Kong, J.Y. Jang, J.S. Han, Y. Ji, J. Lee, J.B. Kim, Lipid droplet protein LID-1 mediates ATGL-1-dependent lipolysis during fasting in Caenorhabditis elegans, Mol. Cell. Biol. 34 (2014) 4165–4176.

[82] I.M. Siddiqah, S.P. Manandhar, S.M. Cocca, T. Hsueh, V. Cervantes, E. Gharakhanian, Yeast ENV9 encodes a conserved lipid droplet (LD) short-chain dehydrogenase involved in LD morphology, Curr. Genet. 63 (6) (2017) 1053–1072.

[83] P.J. Thul, K. Tschapalda, P. Kolkhof, A.R. Thiam, M. Oberer, M. Beller, Lipid droplet subset targeting of the Drosophila protein CG2254/dmLdsdh1, J. Cell Sci. 130 (18) (2017) 3141–3157.

[84] M.L. Casey, P.C. MacDonald, S. Andersson, 17 beta-Hydroxysteroid dehydrogenase type 2: chromosomal assignment and progestin regulation of gene expression in human endometrium, J. Clin. Invest. 94 (1994) 2135–2141.

[85] Y. de Launoit, J. Adamski, Unique multifunctional HSD17B4 gene product: 17beta-hydroxysteroid dehydrogenase 4 and D-3-hydroxyacyl-coenzyme A dehydrogenase/hydratase involved in Zellweger syndrome, J. Mol. Endocrinol. 22 (1999) 227–240.

[86] M.G. Biswas, D.W. Russell, Expression cloning and characterization of oxidative 17beta- and 3alpha-hydroxysteroid dehydrogenases from rat and human prostate, J. Biol. Chem. 272 (1997) 15959–15966.

[87] A. Krazeisen, R. Breitling, K. Imai, S. Fritz, G. Moller, J. Adamski, Determination of cDNA, gene structure and chromosomal localization of the novel human 17beta-hydroxysteroid dehydrogenase type 7(1), FEBS Lett. 460 (1999) 373–379.

[88] J. Villar, J. Celay, M.M. Alonso, M. Rotinen, C. de Miguel, M. Migliaccio, I. Encio, Transcriptional regulation of the human type 8 17beta-hydroxysteroid dehydrogenase gene by C/EBPbeta, J. Steroid Biochem. Mol. Biol. 105 (2007) 131–139.

[89] X.Y. He, G. Merz, Y.Z. Yang, R. Pullakart, P. Mehta, H. Schulz, S.Y. Yang, Function of human brain short chain L-3-hydroxyacyl coenzyme A dehydrogenase in androgen metabolism, Biochim. Biophys. Acta 1484 (2000) 267–277.

[90] V. Luu-The, P. Tremblay, F. Labrie, Characterization of type 12 17beta-hydroxysteroid dehydrogenase, an isoform of type 3 17beta-hydroxysteroid dehydrogenase responsible for estradiol formation in women, Mol. Endocrinol. 20 (2006) 437–443.

[91] R.V. Farese Jr., T.C. Walther, Lipid droplets go nuclear, J. Cell Biol. 212 (2016) 7–8.

[92] J.P. Layerenza, P. González, M.M. García de Bravo, M.P. Polo, M.S. Sisti, A. Ves-Losada, Nuclear lipid droplets: a novel nuclear domain, Biochim. Biophys. Acta (BBA) - Mol. Basis Dis. 1831 (2013) 327–340.

[93] H. Goldfine, Bacterial membranes and lipid packing theory, J. Lipid Res. 25 (1984) 1501–1507.

[94] R. Conde-Alvarez, M.J. Grillo, S.P. Salcedo, M.J. de Miguel, E. Fugier, J.P. Gorvel, I. Moriyon, M. Iriarte, Synthesis of phosphatidylcholine, a typical eukaryotic phospholipid, is necessary for full virulence of the intracellular bacterial parasite Brucella abortus, Cell. Microbiol. 8 (2006) 1322–1335.

[95] Y. Horiguchi, M. Araki, K. Motojima, Identification and characterization of the ER/lipid droplet-targeting sequence in 17beta-hydroxysteroid dehydrogenase type 11, Arch. Biochem. Biophys. 479 (2008) 121–130.

[96] L. Yang, Y. Ding, Y. Chen, S. Zhang, C. Huo, Y. Wang, J. Yu, P. Zhang, H. Na, H. Zhang, et al., The proteomics of lipid droplets: structure, dynamics, and functions of the organelle conserved from bacteria to humans, J. Lipid Res. 53 (2012) 1245–1253.

[97] D. Lohmann, J. Spandl, A. Stevanovic, M. Schoene, J. Philippou-Massier, C. Thiele, Monoubiquitination of ancient ubiquitous protein 1 promotes lipid droplet clustering, PLoS One 8 (2013) e72453.